# 目录

# 1.货物交接清单

## 货物交接清单

需方：郑州大学基础医学院

供方：广州市诚屹进出口有限公司

| 序号 | 设备名称 | 品牌型号 | 数量 | 放置房间 |
|---|---|---|---|---|
| 1 | 3D断层多功能活体光学/CT成像系统 | PerkinElmer IVIS Spectrum CT | 1 | 533 |
| 1.1 | 电脑工作站 | Precision 5820 | 1 | 533 |
| 1.2 | 一体式气体麻醉系统 | RAS-4 | 1 | 533 |
| 2 | 双人生物安全柜 | Thermo Scientific/1389 | 2 | A1-510/527 |
| 3 | 脉动真空灭菌器 | 北京白象/ HS-360 | 1 | A1-133 |

广州市诚屹进出口有限公司

供方负责人：黄意

联系电话：17728161724

郑州大学基础医学院

需方接收人签字：

联系电话：13051575129

日期：2021 年 7 月 30 日

# 1.1 货物交接


## 1.2 货物交接明细

## 1. 3D 断层多功能活体光学/CT 成像系统

<table>
<tr><td>  </td><td> 
</td></tr>
<tr><td>3D 多功能活体光学 CT 成像系统</td><td>铭牌</td></tr>
<tr><td> 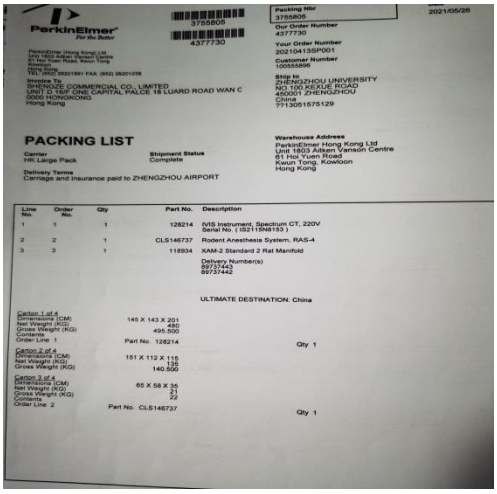
</td><td> 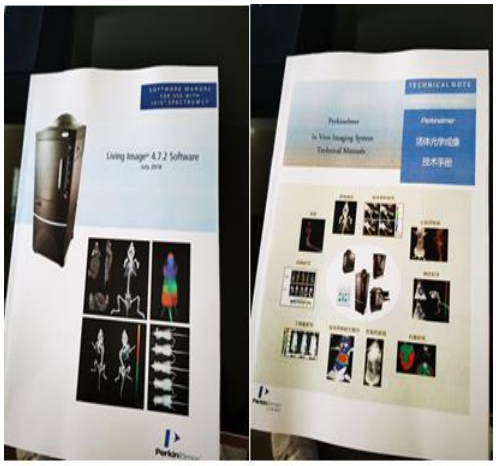
</td></tr>
<tr><td>装箱单</td><td>中英文操作说明书</td></tr>
<tr><td> 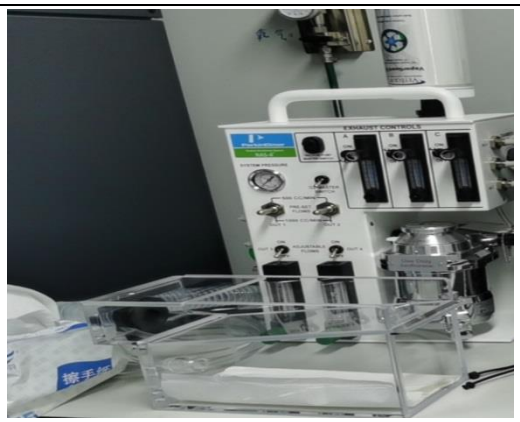 </td><td> 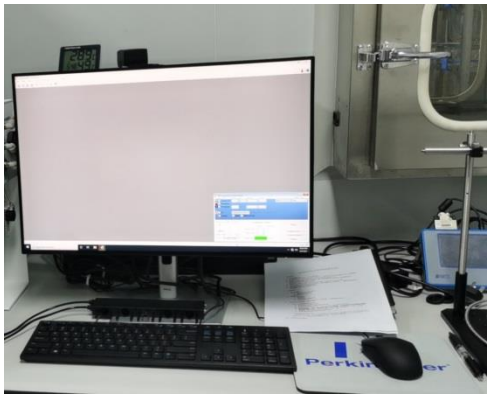 </td></tr>
<tr><td>麻醉机</td><td>电脑工作站</td></tr>
</table>

# 2.双人生物安全柜

双人生物安全柜


铭牌

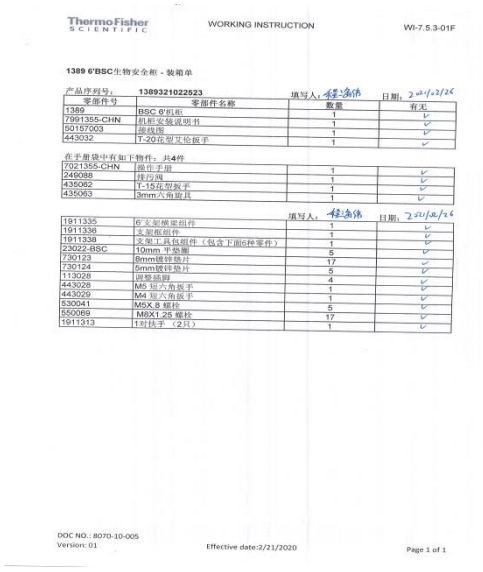

ThermoFisher SCIENTIFIC　WORKING INSTRUCTION　WI-7.5.3-01F

1389 6'BSC生物安全柜 - 装箱单

产品序列号: 1389321022523　填写人: 程海伟　日期: 2021/2/26

| 零部件号 | 零部件名称 | 数量 | 有无 |
|---|---|---|---|
| 1389 | BSC 6'机柜 | 1 | ✓ |
| 7991355-CHN | 机柜安装说明书 | 1 | ✓ |
| 50157003 | 接线图 | 1 | ✓ |
| 443032 | T-20花型艾伦板手 | 1 | ✓ |

在手册袋中有如下物件: 共4件

| | | | |
|---|---|---|---|
| 7021355-CHN | 操作手册 | 1 | ✓ |
| 249088 | 排污阀 | 1 | ✓ |
| 435062 | T-15花型板手 | 1 | ✓ |
| 435063 | 8mm六角扳具 | 1 | ✓ |

填写人: 程海伟　日期: 2021/2/26

| | | | |
|---|---|---|---|
| 1911335 | 6'支架横梁组件 | 1 | ✓ |
| 1911336 | 支架框组件 | 1 | ✓ |
| 1911338 | 支架工具包组件（包含下面6种零件） | 1 | ✓ |
| 23022-BSC | 10mm 平垫圈 | 5 | ✓ |
| 730123 | 8mm镀锌垫片 | 17 | ✓ |
| 730124 | 5mm镀锌垫片 | 5 | ✓ |
| 113028 | 调整脚爪 | 4 | ✓ |
| 443028 | M5 短六角扳手 | 1 | ✓ |
| 443029 | M4 短六角扳手 | 1 | ✓ |
| 530041 | M5X.8 螺栓 | 5 | ✓ |
| 550069 | M8X1.25 螺栓 | 17 | ✓ |
| 1911313 | 1吋扶手（2只） | 1 | ✓ |

DOC NO.: 8070-10-005
Version: 01　Effective date:2/21/2020　Page 1 of 1

装箱单


中英文说明书

# 3.脉动真空灭菌器

脉动真空灭菌器


铭牌

白象医疗 BAIXIANG MEDICAL

编号：BX-Z1-17-4.2.5

装箱单

（HS-360 脉动真空蒸汽灭菌器）

| 序号 | 名称 | 数量 | 单位 | 备注 |
|---|---|---|---|---|
| 1 | 脉动真空蒸汽灭菌器 | 1 | 台 | |
| 2 | 层板 | 2 | 件 | |
| 3 | 搬运车 | 2 | 辆 | |
| 4 | 手动棘轮扳手 | 1 | 套 | |
| 5 | 打印纸 | 5 | 卷 | |
| 6 | BD 测试包 | 5 | 个 | |
| 7 | 132°化学指示卡 | 1 | 盒 | |
| 8 | 灭菌指示胶带 | 1 | 卷 | |
| 9 | 化学指示标签 | 1 | 盒 | |
| 10 | 生物指示剂 | 1 | 盒 | |
| 11 | 说明书 | 1 | 本 | |
| 12 | 维修手册 | 1 | 本 | |
| 13 | 合格证 | 1 | 份 | |
| 14 | 保修卡 | 1 | 份 | |
| 15 | 装箱单 | 1 | 份 | |
| 16 | 验收单 | 2 | 份 | |
| 17 | 设备反馈单 | 1 | 份 | |
| 18 | 用户须知 | 1 | 份 | |
| 19 | 操作指南 | 1 | 份 | |

客户签字：　　工程师：　　检验员：

装箱单

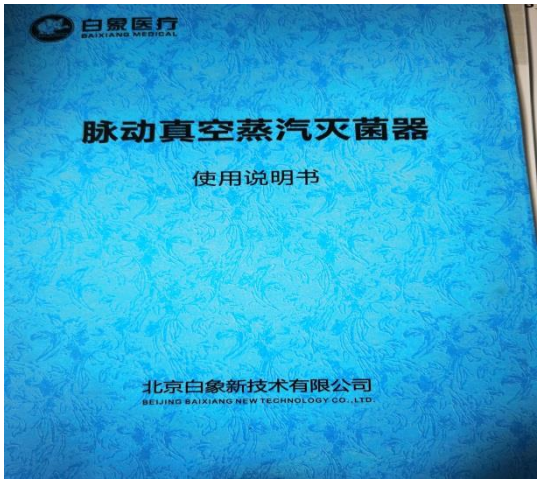


说明书


合格证


保修卡

# 2.设备安装调试报告

## 2.1 设备安装调试报告—3D 断层多功能活体光学/CT 成像系统

PerkinElmer For the Better

表单编号: 17-05-LS-0009 版本 01

### 安装测试表

**仪器名称： IVIS Spectrum CT**

仪器型号： Spectrum CT 仪器序列号： IS2115N8153

用户名称： 郑州大学

地 址： 郑州市中原区科学大道 100 电话/传真： 13051575129

用户姓名： 江冰 服务工程师： 袁举现 日期： 2021-09-02

1、☐ 现场检查环境条件 √

2、☐ 清点货物 √

3、☐ 硬件连接 √

4、☐ 软件连接 √

5、安装测试记录

| 项目 | 标准值 | 实测值 | 结论 |
|---|---|---|---|
| 仪器初始化 | 仪器能正常完成初始化 | 正常 | 合格 |
| 像机成像水平位置校准 | 安装校准工具，成像后圆形的图像处于中心位置。 | 正常 | 合格 |
| 像机成像角度位置校准 | 检查图像水平线与单个老鼠床的中线是否平行，角度偏移小于 2 个像素 | 正常 | 合格 |
| 暗箱漏光测试 | 平均值<50 counts | <23 counts | 合格 |
| 聚焦测试 | Fstop=1 时聚焦良好 | 良好 | 合格 |
| 光子定量校准 | 将测试数据填入 Photon calibration 表格，所有计算结果均显示 pass. | Pass | 合格 |
| QD800 | 荧光模式 EX710,Em800,有正常的 荧光信号. | 正常 | 合格 |
| 滤光片测试 | 选取 80%的正方形的区域，Efficiency 平均值小于 2.0e-5. | 小于 2.0e-5 | 合格 |
| 检查透射荧光光源位置 | 检查透视荧光光源与透射多孔板的孔的位置对齐. | 正常 | 合格 |
| DLIT 成像功能检查 | DLIT 模式能够正常成像 | 正常 | 合格 |
| FLIT 成像功能检查 | FLIT 模式能够正常成像 | 正常 | 合格 |
| 检查 CT 成像位置 | 对专用检查工具成像，CT 图像要与明场图像重合 | 正常 | 合格 |
| CT 成像物体密度检查 | 水密度 标准值 0 ， 偏差值小于±50 | 小于 6 | 合格 |
| | 空气密度 标准值-1000 ， 偏差值小于 | 小于 1 | 合格 |

| | | | |
|---|---|---|---|
| | ±100 | | |
| CT 成像检查 | CT 各模式下能够正常成像，图像无重影. | 正常 | 合格 |
| 载物台加热功能 | 载物台能够正常加热 | 正常 | 合格 |
| 备份校准及检测数据 | 备份仪器的各校准数据及安装测试数据 | 完成 | 完成 |

6、客户培训：

☐ 1、回顾客户仪器安装的性能情况及环境状况。√
☐ 2、简述仪器特点及基本工作原理。√
☐ 3、说明正确的开机顺序及安全操作。√
☐ 4、演示如何启动仪器软件。√
☐ 5、说明如何进行一个简单的样品**拍照**。√
☐ 6、简述图形窗口基本功能。√
☐ 7、说明关机程序。√
☐ 8、说明仪器出现故障时应采取的措施及报修步骤。√

服务电话： 800-820-5046 或 021-60645820

该仪器已经按照标准安装程序完成安装，经测试已达到仪器出厂性能指标，此仪器运作正常并交付客户使用。

工程师签名：

客户签名

# 附：安装调试

对 3D 断层多功能活体光学/CT 成像系统主机与麻醉机及电脑工作站进行连接及调试。

**加固主机零部件**

**连接麻醉机**

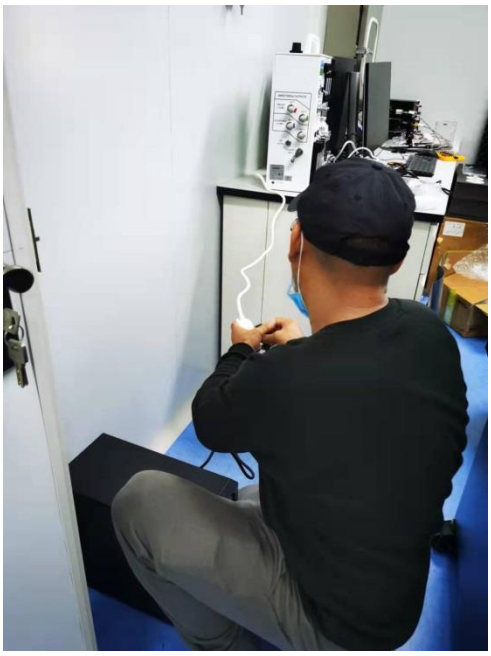

**安装电脑工作站**


**仪器正常运行**

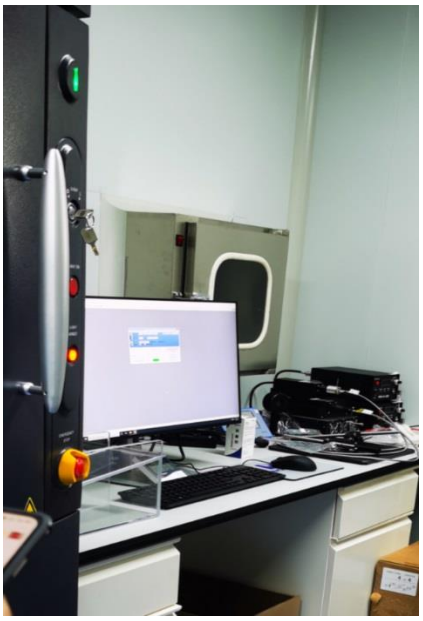

# 2.2 双人生物安全柜安装调试报告

岳鼎科技
YUEDING SCIENTIFIC

## 售后服务报告

| | | | |
|---|---|---|---|
| 客户资料 | 单　位：郑州大学基础医学大楼 | | 工作日期：2021.9.3 |
| | 地　址：郑州市科学大道 | | 合同号： |
| | 联系人：江冰 | | 销售订单号： |
| | 电　话：13051575129 | | 邮　箱： |
| 设备资料 | 机器名称：生物安全柜 | 型号：1389 | 序列号：1389321022823 |
| | 机器名称：生物安全柜 | 型号：1389 | 序列号：1389321022524 |
| | 机器名称： | 型号： | 序列号： |
| | 机器名称： | 型号： | 序列号： |
| | 机器名称： | 型号： | 序列号： |

备注：

服务类型　☑安装服务　□保内服务　□收费服务　□维护　□其它

| | |
|---|---|
| 详情 | 设备故障现象： |
| | 详细工作状况：备件齐全，运行正常，培训完成 |
| | 建议： |

| | |
|---|---|
| 设备上是否粘贴有售后服务电话： | ☑是　□否 |
| 实验室负责人（签名/盖章）：江冰 2021 年 9 月 3 日 | 维修工程师：李明 2021 年 9 月 3 日 |

河南岳鼎科技有限公司
电话：0371-69328688
E-mail：yueding2015@vip.163.com

地址：郑州市东风路丰庆路融海海尚 C 座 808
服务电话：13938485615（24 小时）
13071038987

# 安装调试

安装生物安全柜支架，可调高度。顶部装有紫外灯管。

# 2.3 脉动真空灭菌器安装调试报告

白象医疗
BAIXIANG MEDICAL

## 安装调试报告

（HS-360 脉动真空蒸汽灭菌器）

客户您好！

感谢您选用我公司生产的 HS 系列脉动真空蒸汽灭菌器产品，由我公司委派专业的技术人员为您安装、调试；合格后请贵院（验收意见）填写下列表格。

| | | | |
|---|---|---|---|
| 用户名称 | | 郑州大学基础医学院 | |
| 用户地址 | | 郑州市高新区科学大道100号 | |
| 使用人 | 江水 | 联系电话 | 13051575129 |
| 型号 | SH-360 | 生产 TS 批号 | 蒸汽发生器 TS 批号 |
| 生产日期 | 2021年1月7日 | 安装日期 | 2021年3月17日 |
| 安装工程师 | 刘福平 | 验收日期 | 2021年3月17日 |
| 培训情况 | | 熟练操作☑ 基本会操作☐ 不会操作☐ | |
| 工程师服务态度 | | 非常满意☑ 满 意☐ 不满意☐ | |
| 参加培训人员签字：<br>江水、张帅兵、刘闯 葛梦月 | | | |

白象医疗
BAIXIANG MEDICAL

编号：BX-ZJ-13-4.3-5

## 附表：验收确认内容

| 序号 | 验收确认内容 | 用户确认 | 备注 |
|---|---|---|---|
| 1 | 汽源、水源管道直径是否与灭菌器进汽、进水管道直径相等 | 是☑否☐ | |
| 2 | 汽源管道是否安装有汽源压力表、过滤器、疏水阀或排冷凝水阀 | 是☑否☐ | |
| 3 | 水源管道是否装有水源压力表 | 是☑否☐ | |
| 4 | 总排管是否由“1/2”变为1或“3/4”管路排出 | 是☑否☐ | |
| 5 | 设备是否安全接地 | 是☑否☐ | |
| 6 | 是否检查蒸汽源压力（0.3～0.6MPa）、水源压力（0.1～0.3MPa） | 是☑否☐ | |
| 7 | 工作时蒸汽源压力是否大于0.3MPa，水源是否大于0.1MPa，空气源压力是否大于0.4MPa | 是☑否☐ | |
| 8 | 工作时，压缩空气源是否在0.4～0.8MPa之间 | 是☑否☐ | |
| 9 | 设备工作时温度最高是 121 ℃ | 是☑否☐ | |
| 10 | 设备灭菌时内室压力是 0.115 MPa | 是☑否☐ | |
| 11 | 设备灭菌时夹套压力是 0.21 MPa | 是☑否☐ | |
| 12 | 程序是否运行正常（包含B-D测试、液体程序、真空程序） | 是☑否☐ | |
| 13 | 设备是否有漏气现象？如有是否解决 | 是☑否☐ | |
| 14 | 真空泵是否能抽至设定负压及运行是否正常（仅适用脉动真空柜） | 是☑否☐ | |
| 15 | 设备经调试后是否正常通过B-D测试（注：仅适用脉动真空柜） | 是☑否☐ | |
| 16 | 在调试人员的指导下是否能熟练地对设备参数进行设置 | 是☑否☐ | |
| 17 | 调试人员是否指导设备操作至熟练为止 | 是☑否☐ | |
| 18 | 调试员是否对设备的整个过程及方式作了详细讲解 | 是☑否☐ | |
| 19 | 调试人员是否对灭菌器的常规故障及排除方法作了详细介绍 | 是☑否☐ | |

一式二份：公司存档一份、客户存档一份。

# 安装调试

对机器内部部件进行检测和减压阀及安全阀的安装。


## 压力表校正完成

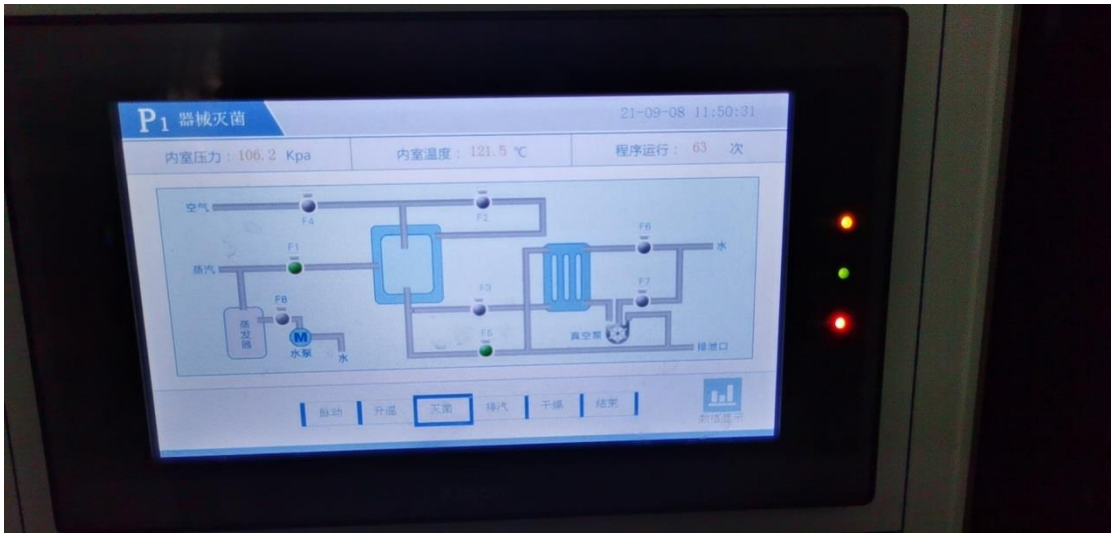

# 3.设备性能测试报告

## 3.1 3D 断层多功能活体光学/CT 成像系统性能测试报告

PerkinElmer
For the Better

### 3D 断层多功能活体光学/CT 成像系统

# 测
# 试
# 报
# 告

用户：郑州大学基础医学院　　地址：郑州市高新区科学大道 100 号

仪器品牌：PerkinElmer　仪器型号：IVIS Spectrum CT

测试工程师：郝盼　　日期：2021 年 7 月 30 日

工程师签字确认：　　使用人签字确认：

日期：郝盼　　日期：2021.7.30


图 1

1. 测试内容：此仪器配置高灵敏度的生物发光及荧光二维成像功能。

实际测试结果：如图 1 所示，以上图片显示测试结果符合参数中性能指标要求，满足实验需求。

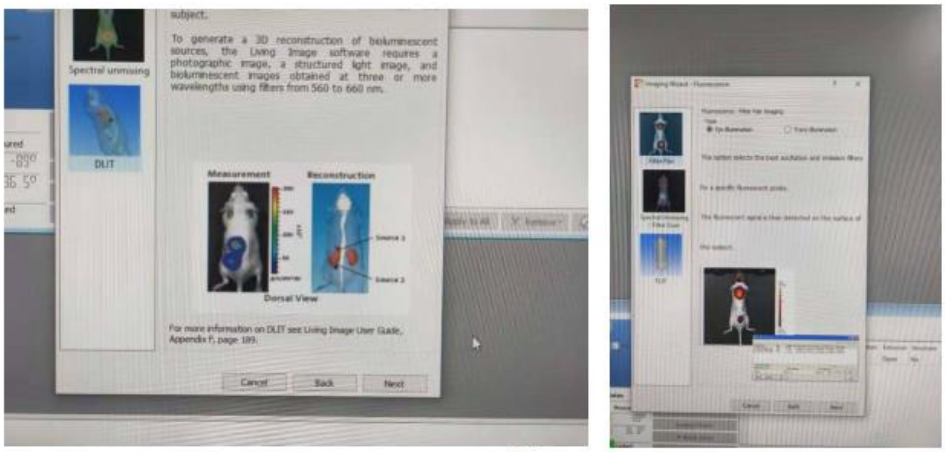


图 2-3

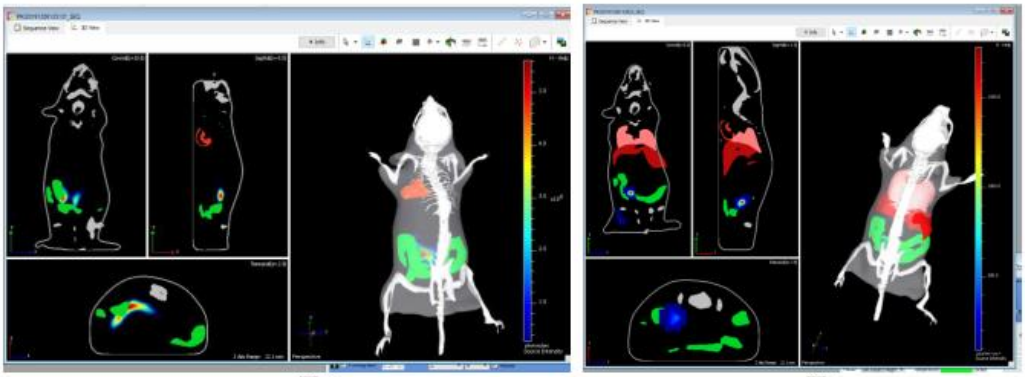

图 4　　图 5

2.测试内容：此仪器配备专利的生物发光及荧光三维成像功能。

实际测试结果：如图 2-3、图 4、图 5 所示，此仪器具备生物发光及荧光的三维光学成像功能，测试结果符合参数中性能指标要求，满足实验需求。

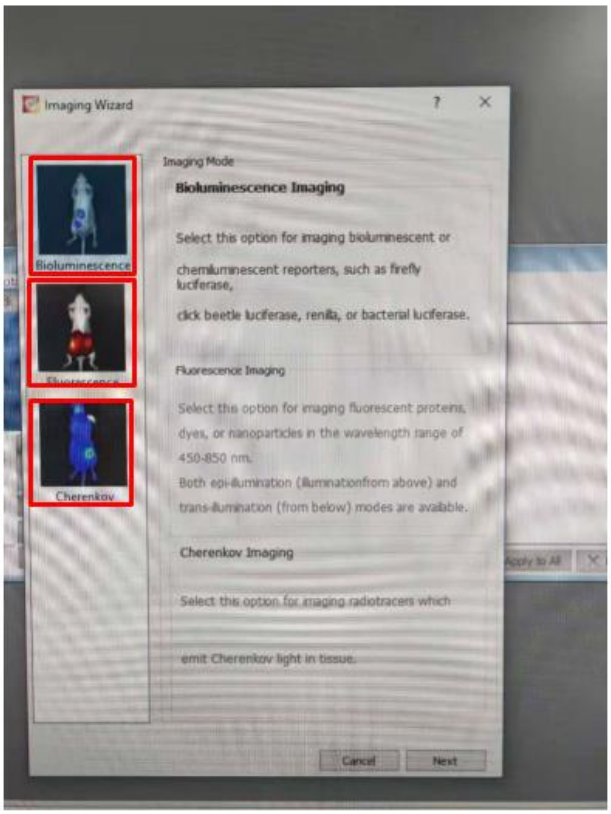


图 6

3.测试内容：基于切伦科夫辐射原理的放射性同位素成像功能。

实际测试结果：如图 6 所示，以上图片显示测试结果符合参数中性能指标要求，满足实验需求。

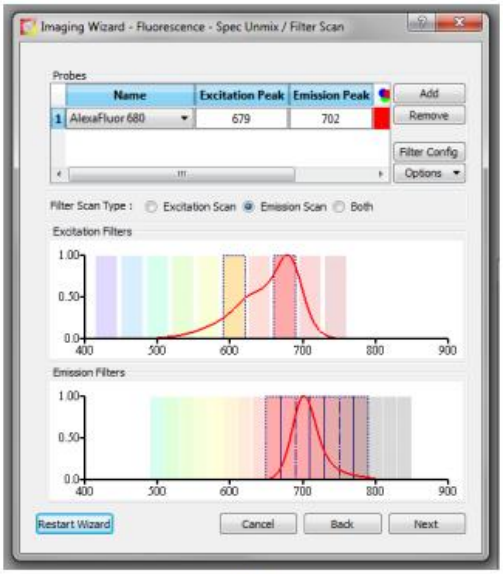


图 7

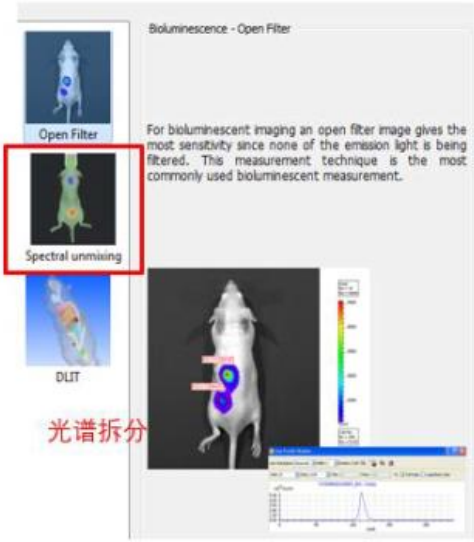


图 8

4．测试内容，软件可提供超高精细度的光谱拆分功能。提供 18 个发射光滤光片及 10 个激发光滤光片。可进行高精度光谱扫描和拆分。软件设置有超过 20 个已有染料或荧光蛋白的光谱库。以上可极大减少传统光谱扫描精度不高或无法获取特异性标曲的问题。（图 7-8）

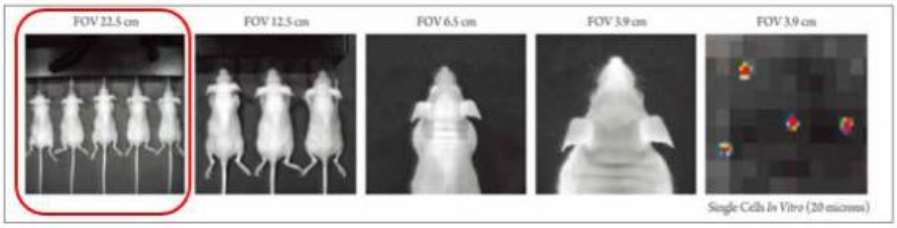


图 9

5．测试内容：配置高通量成像能力，可同时成像 5 只小鼠。

实际测试结果：如图 9 成像视野范围可调，最大视野能够满足至少 5 只小鼠同时成像。

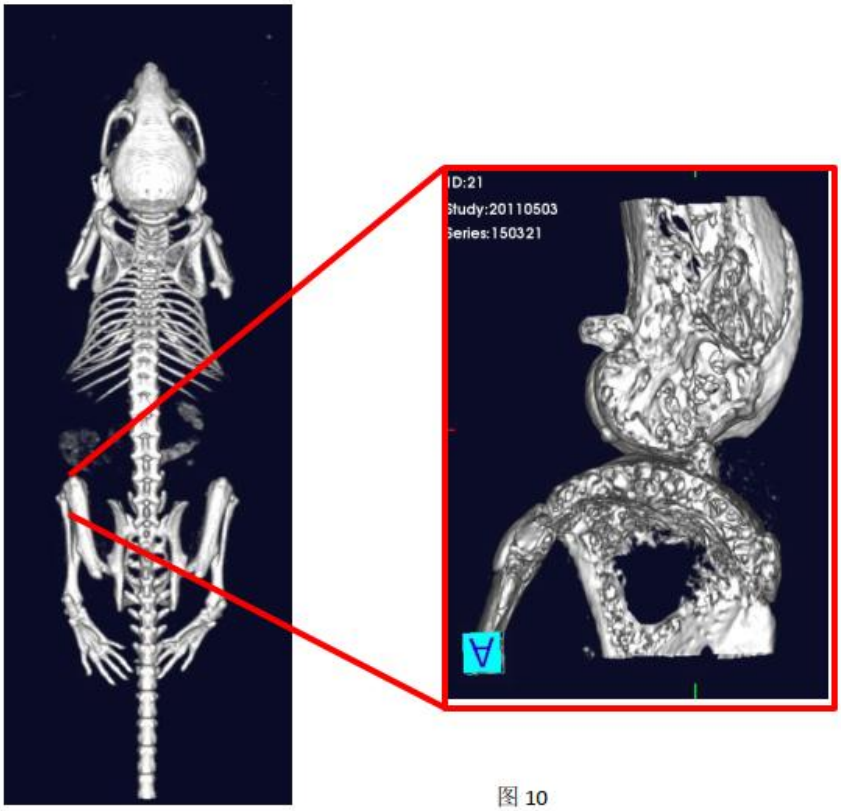


图 10

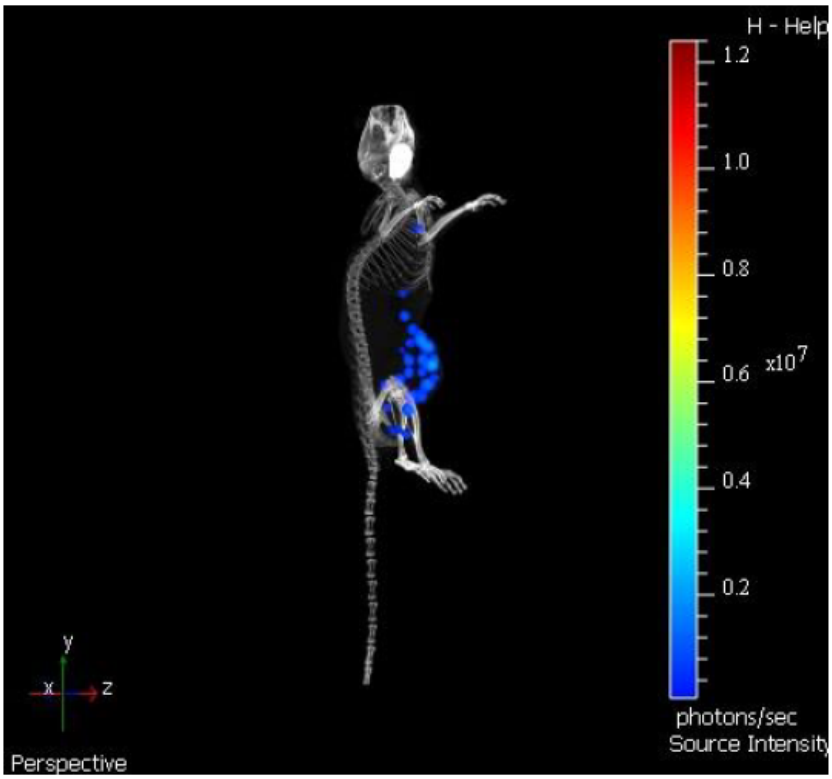


图 11

6.测试内容，配置高级三维光学成像功能，能够获得成像动物横断面、矢状面及冠状面任意层面的光学信号图像及三维重建影像，能够对信号源体积、深度、强度进行三维定量分析。

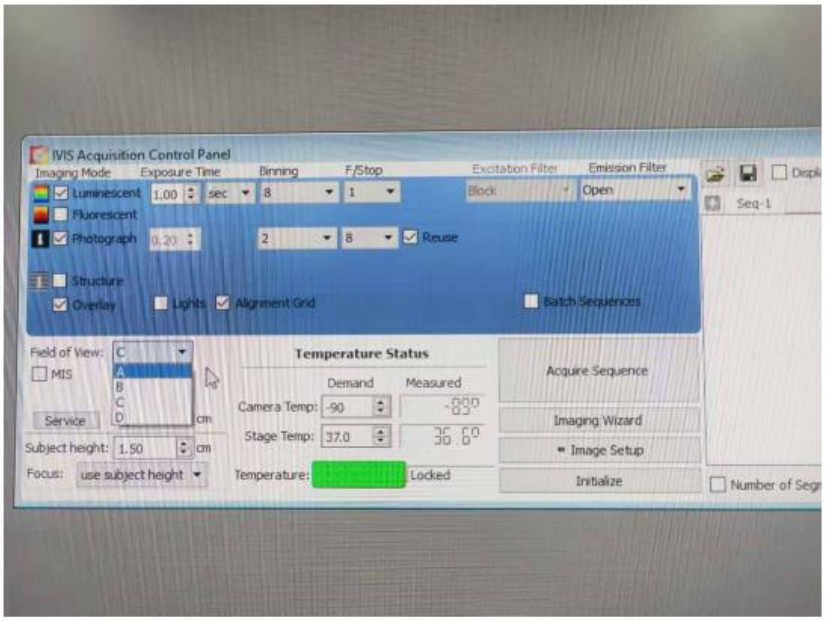


7. 测试内容：此仪器探测器采用顶置式背照射、背部薄化科学一级 CCD 相机，工作温度达到绝对-90℃，软件中相机的温度可视化。

实际测试结果：如图所示，探测器工作温度可达到绝对-90℃，并在软件中实时显示温度。测试结果符合参数中性能指标要求，满足实验需求。

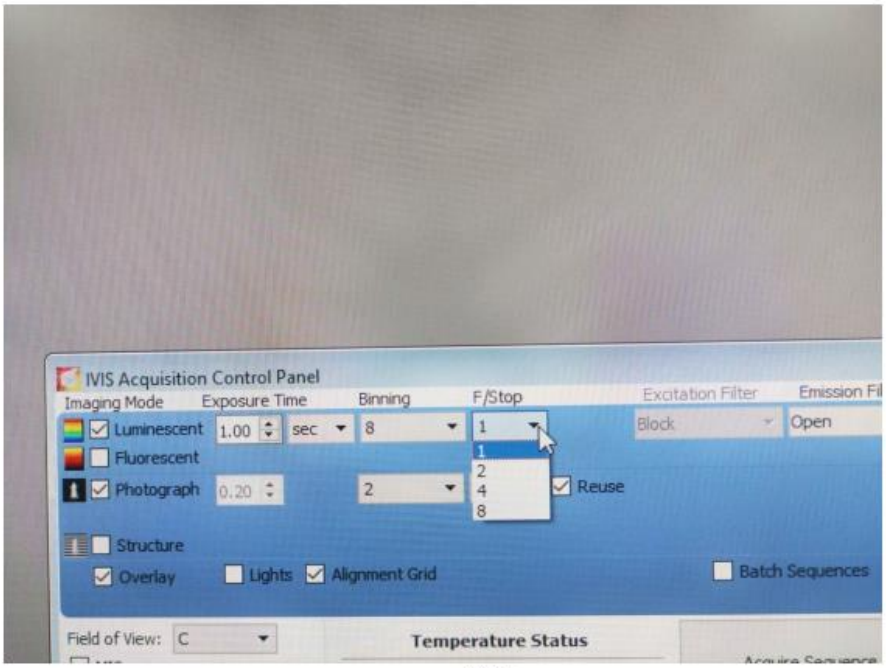


图 13

8.测试内容：相机采用高品质的定焦镜头，最大光圈达 f/1。

实际测试结果：如图所示，相机的光圈可选，最大光圈可达 f/1，符合参数中性能指标要求，满足实验需求。

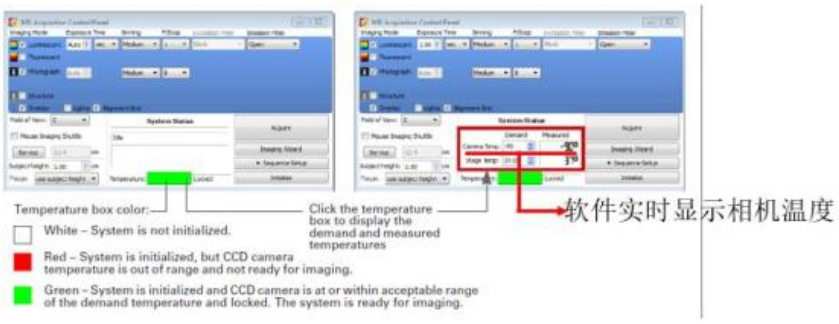


图 14

| | |
|---|---|
| Camera Sensor | Back-thinned, back-illuminated Grade 1 CCD |
| CCD Size | 2.7 x 2.7 cm |
| Imaging Pixels | 2048 x 2048 |
| Quantum Efficiency | > 85% 500 - 700 nm; > 30% 400 - 900 nm |
| Pixel Size | 13.5 microns |
| Min. Detectable Radiance | 70 photons/s/sr/cm² |
| Min. Field of View (FOV) | 3.9 x 3.9 cm |
| Max. Field of View (FOV) | 23 cm x 23 cm |
| Min. Image Pixel Resolution | 20 microns |
| Lens | f/1 - f/8; 1.5 x, 2.5 x, 5 x, 8.7 x magnifications |
| Read Noise | < 3 electrons for bin = 1, 2, 4; < 5 electrons for bin = 8, 16 |
| Dark Current (Typical) | < 100 electrons/s/cm² |

图 15

9.测试内容：满足选择系统最小检测光子数 70 光子/秒/弧度/平方厘米，检测灵敏度达到可检测小鼠皮下 10 个生物发光细胞。（如图 14-15）

| Features | IVIS SpectrumBL | IVIS Spectrum | IVIS SpectrumCT |
|---|---|---|---|
| Animal Capacity | 10 mice | 5 mice | 5 mice |
| Bioluminescence | ✓ | ✓ | ✓ |
| Fluorescence | | ✓ | ✓ |
| Full Spectral Tunability | | ✓ | ✓ |
| Epi-Illumination | | ✓ | ✓ |
| Trans-Illumination | | ✓ | ✓ |
| 3D Fluorescence Tomography | | ✓ | ✓ |
| 3D Bioluminescence Tomography | ✓ | ✓ | ✓ |
| Quantification | ✓ | ✓ | ✓ |
| Absolute Calibration | ✓ | ✓ | ✓ |
| 3D Multimodal Co-Registration (PET, CT, MRI) | ✓ | ✓ | ✓ |
| Integrated X-Ray and microCT | | | ✓ |
| Compute Pure Spectrum - Spectral Unmixing | | ✓ | ✓ |
| Optimized NIR Excitation Lightsource | N/A | Extended NIR Range 150W Tungsten EKE | |

图 16

10. 荧光光源采用长寿命高效金属卤素灯，功率不低于 150 瓦；（如图 16）

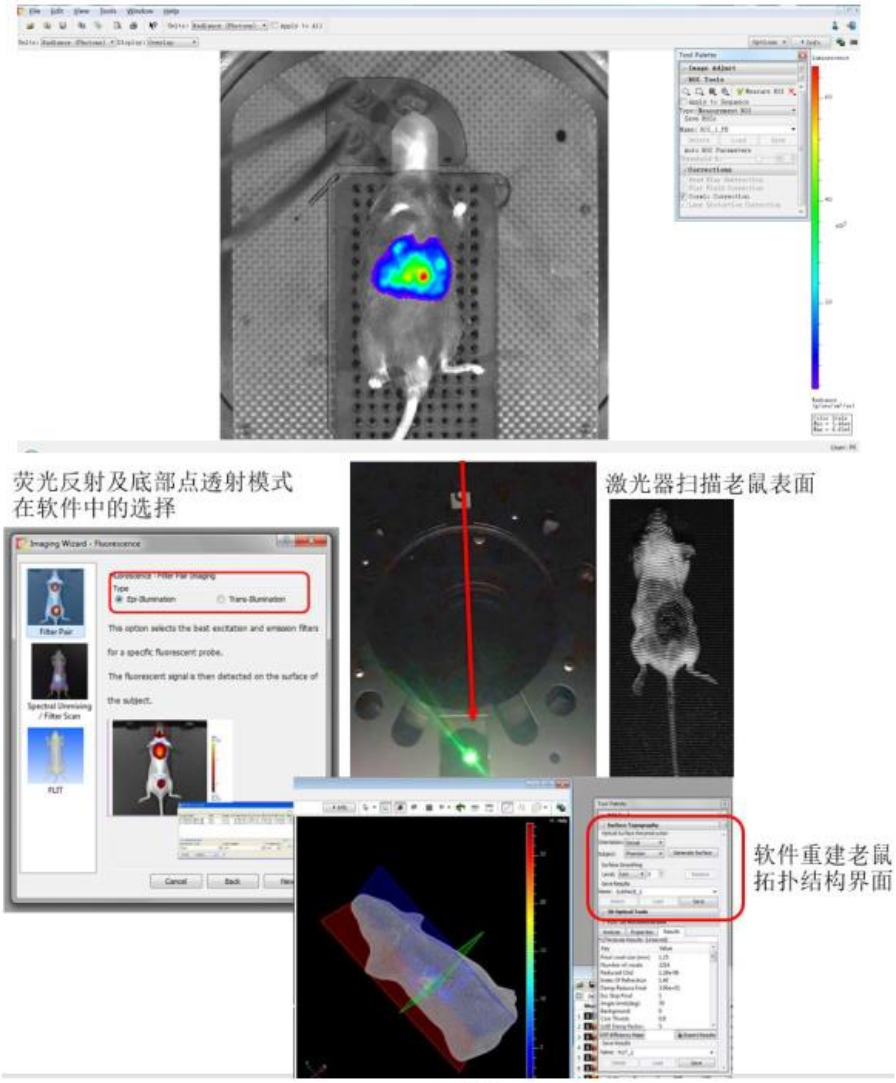


图 17

11. 同时配置荧光反射及底部点透射光路的产品；配置荧光和生物发光透射光路成像模式。（图 17）

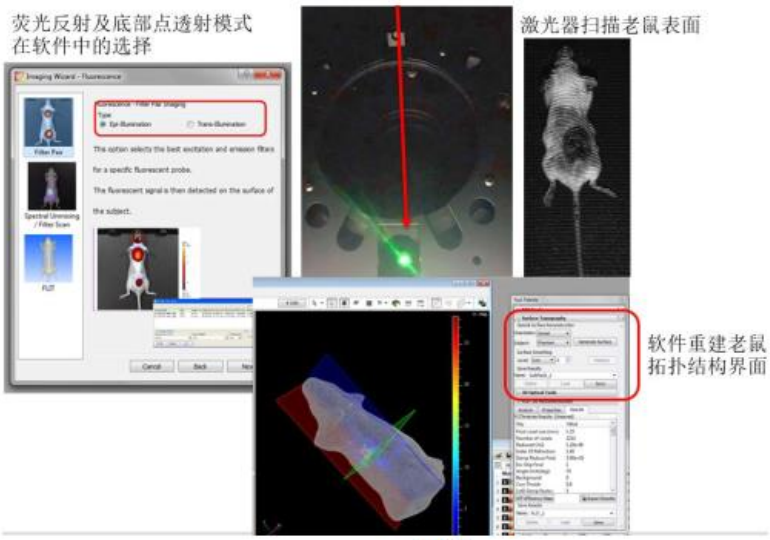


图 18

12.测试内容：此仪器具备激光扫描器，用于三维成像时动物体表拓扑结构的绘制。

实际测试结果：如图 18 所示，此仪器具备激光扫描器，测试结果符合性能指标要求，满足实验需求。

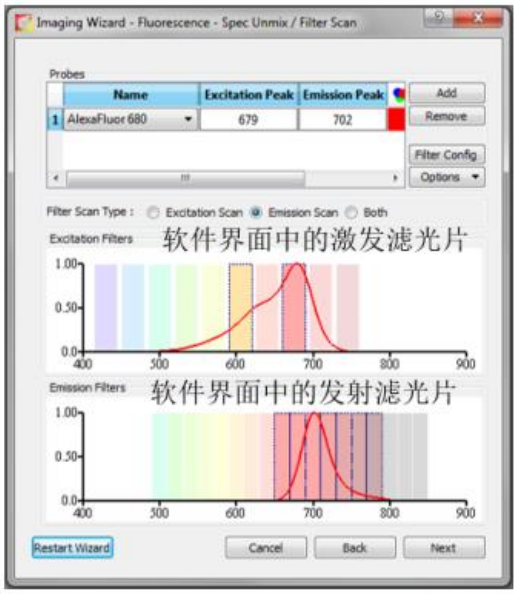


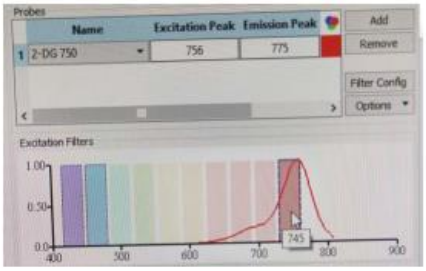


图 19-20

13. 测试内容：此仪器标配 10 个激发光滤色片。

实际测试结果：如图 19-20 所示，此仪器配备 10 个激发滤色片，激发波长范围 430nm-745nm。测试结果符合参数性能指标要求，满足实验需求。

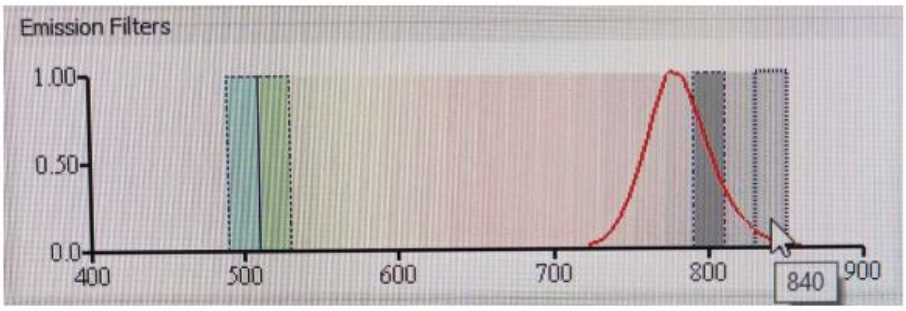


图 21

14. 测试内容：此仪器标配 18 个激发光滤色片。

实际测试结果：如图 21 所示，此仪器配备 18 个激发滤色片，激发波长范围 500-840nm。测试结果符合参数性能指标要求，满足实验需求。

图 22

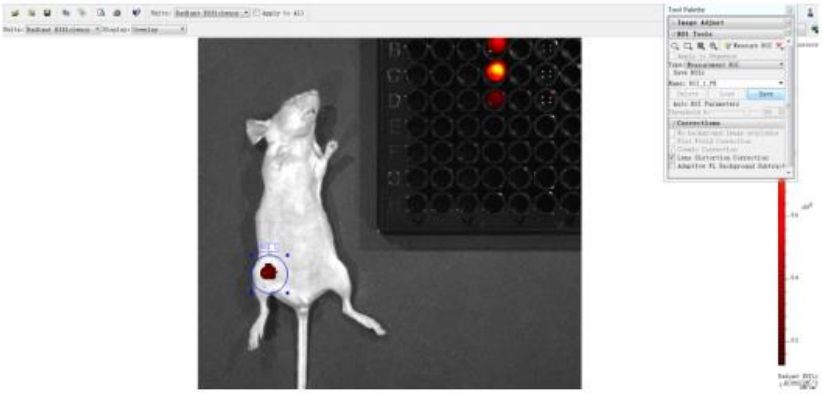

图 22

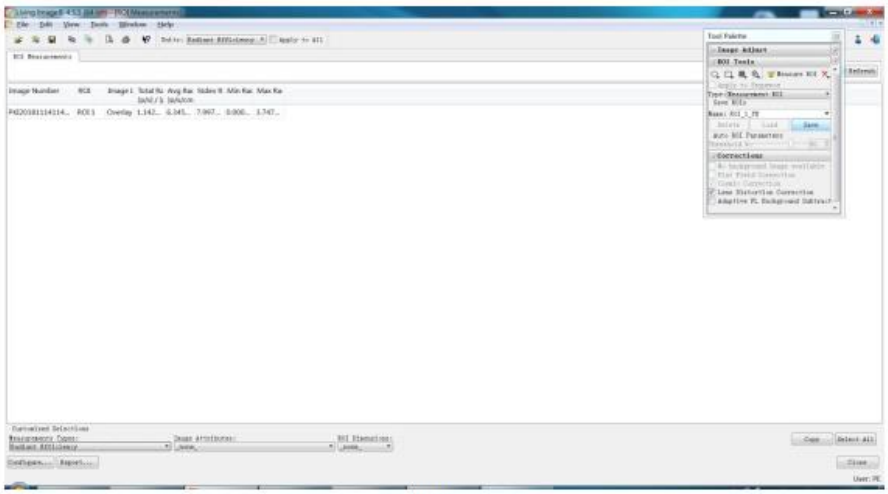

图 22

15.测试内容：此仪器具备荧光光谱分离功能。

实际测试结果：如图 22 所示，此仪器具备荧光光谱分离功能，可去除背景荧光信号。测试结果符合参数性能指标要求，满足实验需求。

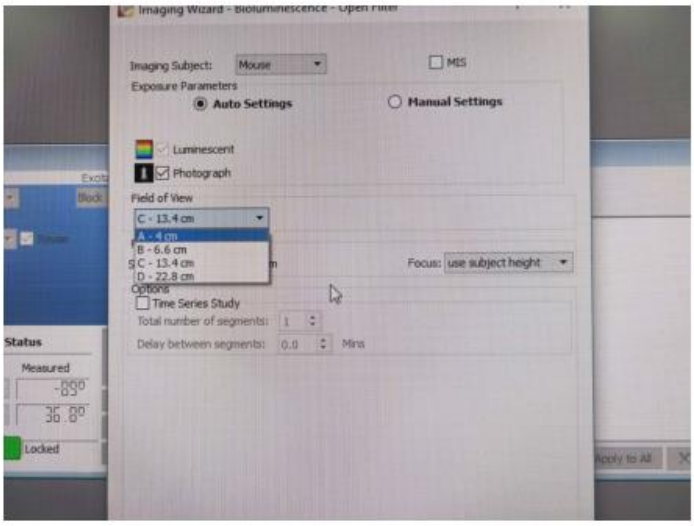


图 23

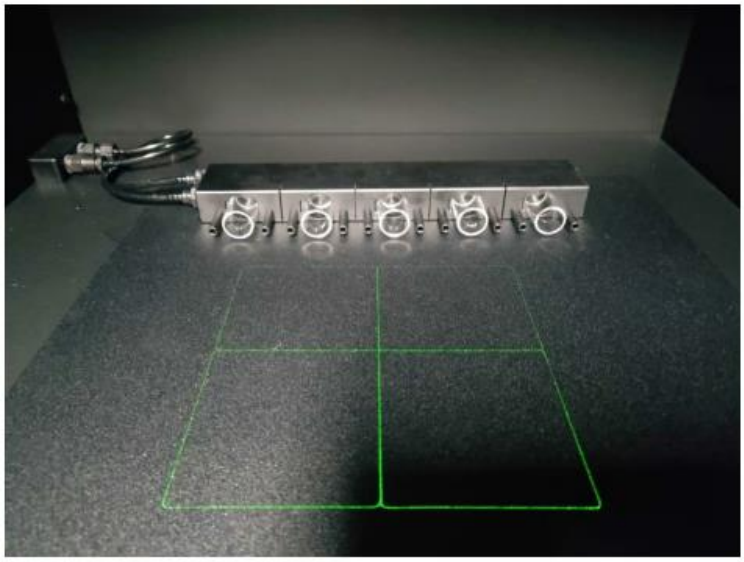

图 24

16.测试内容：此仪器视野范围最大 23cm x 23cm。

实际测试结果：如图 23-24 所示，此仪器成像视野范围可调，最大成像视野范围为 23cm x 23cm。测试结果符合参数性能指标要求，满足

实验需求。

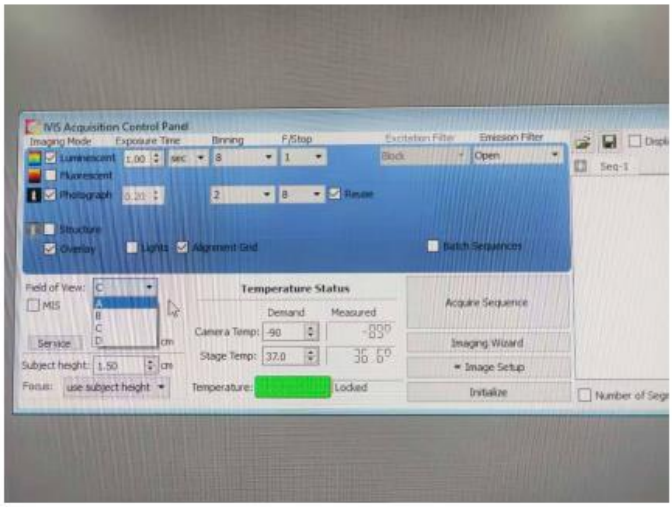


图 25

17.测试内容：动物载物台温度可控(20-40℃)，且即时温度可通过软件显示。

实际测试结果：如图 25 所示，软件可控制动物载物台温度到 37℃。测试结果符合参数性能指标要求，满足实验需求。

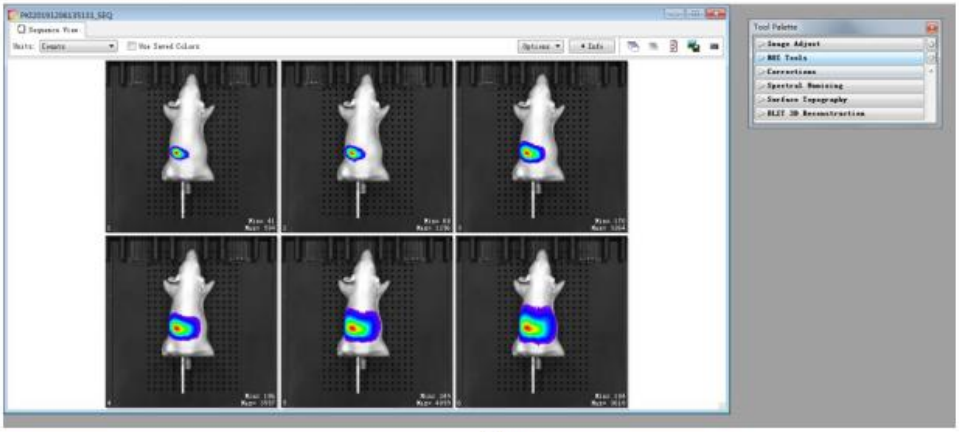


图 26

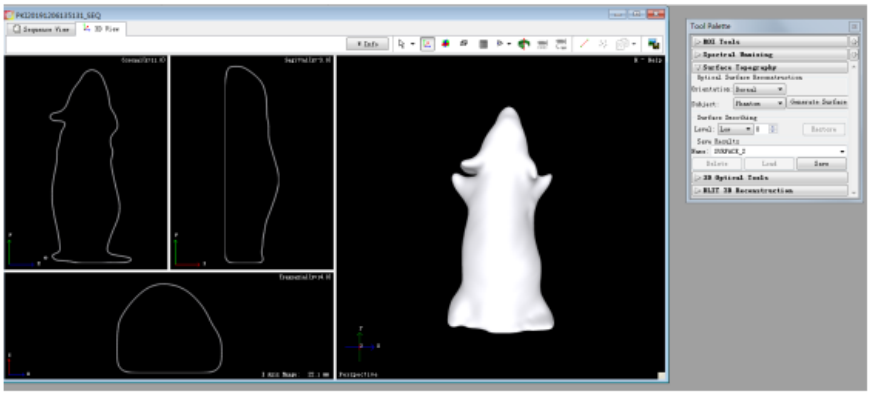

图 27

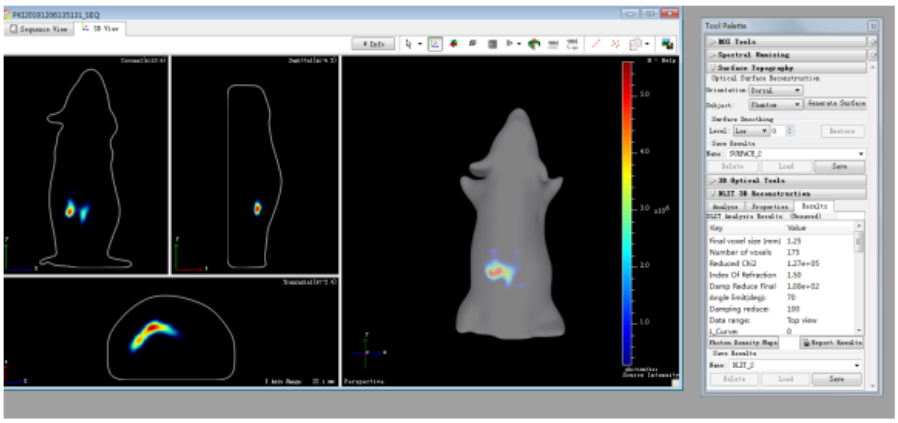

图 28

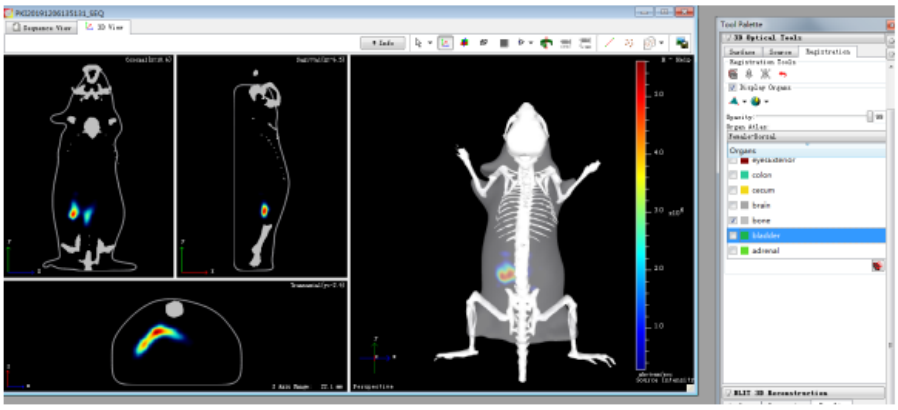

图 29

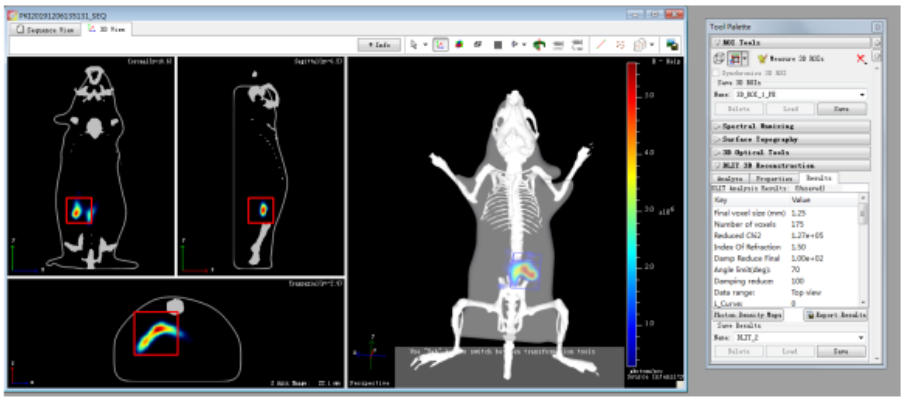

图 30

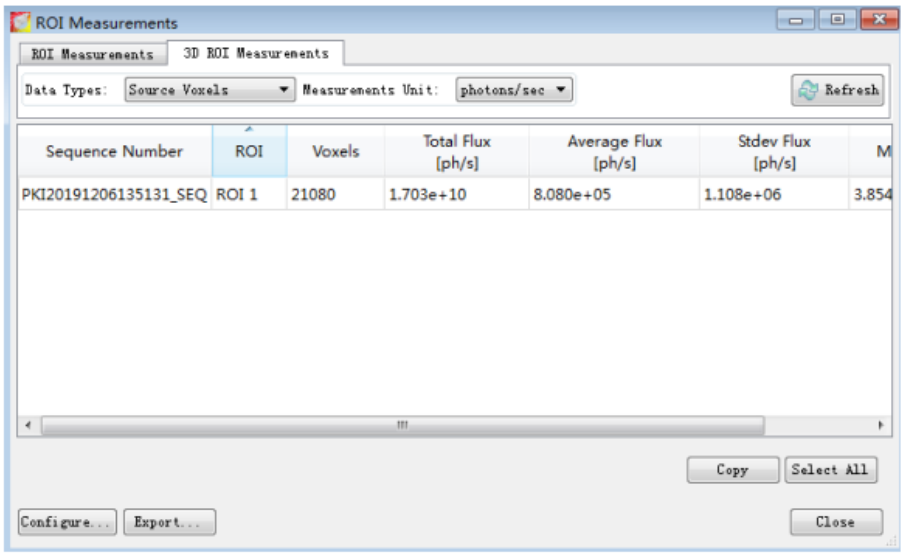


图 31

18.测试内容：标配软件包含图像获取及数据分析模块，具备生物发光结果定量方法，能给出光学信号在体内的深度、发光体积、定位、三维发光强度等三维定量信息。

实际测试结果：如图 26-31 所示，此仪器配备软件包含图像获取及数据分析模块，具备生物发光结果定量方法，能给出光学信号在体内的深度、发光体积、定位、三维发光强度等三维定量信息。测试结果符合参数性能指标要求，满足实验需求。


图 32

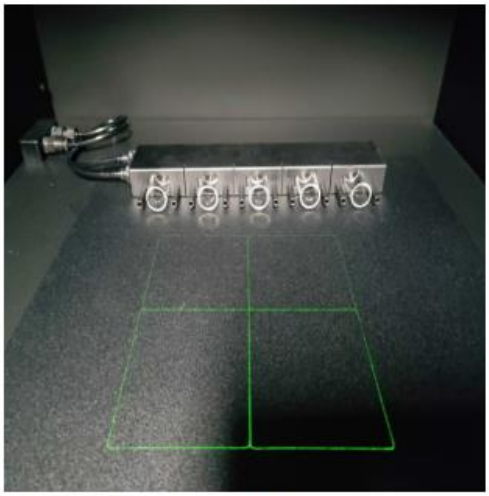

图 33

19. 测试目标：此仪器具备气体麻醉系统，蒸发罐、真空泵、流量控制、尾气吸收等装置。

实际测试结果：如图 32-33 所示，仪器具备气体麻醉系统，蒸发罐、真空泵、流量控制、尾气吸收等装置均为一体化集成，且具备预麻醉盒，用于小鼠成像前的预麻醉处理，可同时麻醉 5 只小鼠。测试结果符合参数性能指标要求，满足实验需求。

# 20 检测灵敏度证明文献 1

OPEN ACCESS Freely available online

PLoS one

## Non-Invasive Detection of a Small Number of Bioluminescent Cancer Cells *In Vivo*

**Jae-Beom Kim[1]*, Konnie Urban[1], Edward Cochran[3], Steve Lee[1], Angel Ang[1], Bradley Rice[1], Adam Bata[2], Kenneth Campbell[2], Richard Coffee[2], Alex Gorodinsky[2], Zhan Lu[2], He Zhou[3], Takashi Kei Kishimoto[3], Peter Lassota[1]***

**1** Caliper Life Sciences Inc., Alameda, California, United States of America, **2** Caliper Life Sciences Inc., Cranbury, New Jersey, United States of America, **3** Momenta Pharmaceuticals Inc., Cambridge, Massachusetts, United States of America

**Abstract**

Early detection of tumors can significantly improve the outcome of tumor treatment. One of the most frequently asked questions in cancer imaging is how many cells can be detected non-invasively in a live animal. Although many factors limit such detection, increasing the light emission from cells is one of the most effective ways of overcoming these limitations. Here, we describe development and utilization of a lentiviral vector containing enhanced firefly luciferase (*luc2*) gene. The resulting single cell clones of the mouse mammary gland tumor (4T1-luc2) showed stable light emission in the range of 10,000 photons/sec/cell. In some cases individual 4T1-luc2 cells inserted under the skin of a *nu/nu* mouse could be detected non-invasively using a cooled CCD camera in some cases. In addition, we showed that only few cells are needed to develop tumors in these mice and tumor progression can be monitored right after the cells are implanted. Significantly higher luciferase activity in these cells allowed us to detect micrometastases in both, syngeneic Balb/c and *nu/nu* mice.

**Citation:** Kim J-B, Urban K, Cochran E, Lee S, Ang A, et al. (2010) Non-Invasive Detection of a Small Number of Bioluminescent Cancer Cells *In Vivo*. PLoS ONE 5(2): e9364. doi:10.1371/journal.pone.0009364

**Editor:** Alexander Swarbrick, Garvan Institute of Medical Research, Australia

**Received** May 12, 2009; **Accepted** January 2, 2010; **Published** February 23, 2010



**Funding:** This work was funded internally at Caliper Life Sciences and Momenta Pharmaceuticals. The funders provided reagents, research space, and resources for this study. However, authors are solely involved in study design, data collection and analyses, or preparation of the manuscript. Caliper Life Sciences and Momenta Biopharma agreed to publish these data in a scientific journal. The funders had no role in study design, data collection and analysis, decision to publish, or preparation of the manuscript.

**Competing Interests:** Jae-Beom Kim, Konnie Urban, Steve Lee, Bradley Rice, Adam Bata, Kenneth Campbell, Richard Coffee, Alex Gorodinsky, Zhan Lu and Peter Lassota are employees of Caliper Life Sciences. He Zhou, Edward Cochran and Takashi Kei Kishimoto are employees of Momenta Pharmaceuticals Inc. The authors agree to PLoS One Policy on data sharing policies. There is no patent application filed using the data obtained from this study.

* E-mail: jae.kim@caliperls.com (J-BK); peter.lassota@caliperls.com (PL)

### Introduction

Detection of tumors at early stages is critical for effective tumor treatment and for studying tumorigenesis[1,2,3]. Traditionally, tumor growth was assessed by using mechanical or electronic calipers to take physical measurements of subcutaneous human tumors growing in immunocompromised mice[4]. This method is suitable, however, only for palpable tumors growing under the skin of the animals. Deeper tumor masses, such as osteosarcomas encapsulated by the bone, are not amenable to direct physical measurements. Even in subcutaneous models, tumor burdens may not be accurately quantified using physical measurements because edema and necrotic centers will contribute to the increase in tumor size[5]. Orthotopic solid tumor models circumvent these obstacles and allow fairly accurate assessment of tumor burdens by weighing the excised, "cleaned" tumors after the animals are sacrificed. Classical orthotopic models are impractical for evaluation of compounds' efficacy since they require large numbers of animals to be sacrificed at each time point. Similarly, identification of tumors and quantification of tumor burden in models of metastasis demand exhaustive and tedious histological analyses[6,7,8].

Non-invasive whole body bioluminescence imaging (BLI) allows repeated, real-time *in vivo* monitoring of tumor growth in experimental animals, regardless of tumor locations. In contrast to fluorescence, BLI exhibits minimal background signals from the animal tissues[9]. Therefore, BLI can detect relatively weak signals with high signal to background ratio. Due to its versatility, BLI has been adopted to study preclinical efficacy of drug candidates[10,11,12,13] as well as various aspects of mammalian biology via reporter assays[14,15].

Recently, firefly (*Photinus pyralis*) luciferase was re-engineered to further optimize its expression in mammalian cells. Compared to previous generations of luciferase, the new version (*luc2*) delivers more than a four-fold increase in light emission which was achieved by codon optimization and removal of potential transcription factor binding sites[16]. We postulated that individual cancer cells could be detected *in vivo* by harnessing the increased bioluminescence of *luc2*. To that end, we engineered a lentiviral vector where *luc2* expression is driven via the human ubiquitin C promoter[17]. The construct was then stably transfected into the 4T1 mouse mammary tumor cell line[18,19]. Several stable, single-cell clones (4T1-luc2) were subsequently isolated with light emission in the range of 10,000 photons/sec/cell. Here, we report that, at least in some cases, detection of a single cancer cell *in vivo* using one of these luc-2 labeled clones was achieved. We also show development of tumors from only few cells implanted into *nu/nu* mice and detection of metastases in syngeneic Balb/c mice. To our best knowledge, this is the first report of detection of a single bioluminescent cell *in vivo* using a

non-invasive imaging method. Such bright cells can be effectively used to monitor efficacy of drug candidates in models of metastasis and orthotopic tumor models, to track metastatic migration of cancer cells, and can be also utilized to accurately ascertain whether any residual disease remains following the treatment.

## Results

### Generation of a Lentiviral Vector System and Stable 4T1-luc2 Cell Lines

A lentiviral vector containing the firefly *luc2* gene conjugated to a human ubiquitin C promoter was constructed to generate stable bioluminescent cancer cell lines[16,17,18]. Mouse mammary tumor 4T1 cells were then transfected with the lentiviral vector and stable clones were selected using puromycin (4T1-luc2). Eight clones were chosen for further analyses and their luciferase activities were monitored for four weeks without selection marker. Although there were variations among the clones, the majority of them clones emitted more than 3,000 photons/sec/cell of light. Considering that most cell lines labeled with previous generations of luciferase emit less than 250 photons/sec/cell, our luc2 clones exhibited considerably higher level of light emission[20]. Surprisingly, one clone (C26) initially emitted as much as 52,000 photons/sec/cell but its light emission decreased to 6,400 photons/sec/cell after four weeks (Figure S1A). To confirm that no alteration of cellular physiology occurred during the labeling/cloning process, we compared the clones to the original parental 4T1 cells on several different levels. First, we examined growth patterns. From the eight initially selected clones, we chose two lines (C27 and C38) and compared their growth patterns to the parental 4T1 cells. Both lines had similar doubling times to the parental cells (12.6 hour doubling time for both clones, versus 12.0 hours for the original 4T1 cells).

We also examined other critical parameters of cellular physiology, including effects of ATP consumption. Since luciferase uses one molecule of ATP to produce each photon of light, high levels of light emission could be detrimental to the cell's metabolism due to the depletion of the its ATP pool. To test whether the high light production affects cell physiology, we observed cell growth for four days in the presence of high concentrations of the luciferase substrate, D-luciferin (150 and 300 μg/ml/day). The results demonstrated that, in the presence of D-luciferin, 4T1-luc2 clones showed similar growth patterns to those of cells cultured without D-luciferin and to the parental 4T1 cells (Figure S1B,C,D). This suggests that 4T1-luc2 cells can endure consumption of the ATP required for the high light emission without a significant effect on the cell's ATP pool.

Since clone C26 showed decreasing luciferase activity over time, we attempted the second round of limited dilution single cell cloning from the original mixed population. Four bright clones were selected and their luciferase activities (light emission) were monitored for six weeks without selection pressure (Figure 1A,B). All clones initially produced more than 40,000 photons/sec/cell; then the light emission declined to 10,000 photons/sec/cell, and stabilized at that level. It remained stable for four weeks in the absence of puromycin (Figure 1B). From these clones, the 1A4 clone (4T1-luc2-1A4) was selected for further studies. The growth pattern of the 4T1-luc2-1A4 was comparable to that of the parental 4T1 cells in the presence, or absence of D-luciferin (Figure 1C,D,E). To address the cause of the initial decrease of light emission in 4T1-luc2-1A4 clone, we performed limited dilution culture in 96-well plates. When cells grew to about 25% confluency, we examined luciferase expression by bioluminescent imaging. Every well containing cells showed luciferase activity. These results indicate that the initial decrease of luciferase activity was not due to the loss of luciferase expression in some cells of the clone (Figure S2).

### Non-Invasive Detection of Small Numbers of Cells in *nu/nu* Mice

Because 4T1-luc2 cells showed extremely high light emission, we next attempted to detect small numbers of these cells *in vivo*. Initially, the 4T1-luc2-1A4 cells were prepared using a serial dilution method and were implanted into both flanks of the female nu/nu mice (Figure 2). Different numbers of cells were implanted at each implantation sites. Six implantations were performed for each number of cells (3, 5, 10, and 50 cells). Bioluminescence images were taken immediately after the implantations. Using a highly sensitive cooled CCD camera, we were able to detect as few as 3 cells in the flank implantation (Figure 2A-D, red dotted circles). In some instances, however, we did not detect any meaningful signals from the sites of implantation (Fig 2A-D, yellow dotted circles). This could be attributed to cell death immediately after implantation or to inherent variability of the serial dilution method when the intended number of cells is very small (Fig 2A-D, yellow circles). Separately, we took PC3M-luc-C6 which was one of the brightest cell lines (~250 photons/sec/cell) generated by us thus far (using multiple rounds of transfections by pGL3) and compared it with 4T1-luc2-1A4 cells, by implanting both into SCID-bg mice (Figure S3). The results illustrate that the bioluminescent signals from $10^7$ 4T1-luc2-1A4 cells in furry mice was easily detectable, while no signal was detected from the same number of PC3M-luc-C6 cells.

Six hours after the implantations, we re-imaged the same set of animals (Fig 2E-H). As expected, based on the hostile post-implantation environment, 4 sites of the 10- and 50 cell implantation sites lost their initial bioluminescent signals (Fig 2G,H). Surprisingly, however, we were able to detect signals from 3- and 5 cell implantation sites (Figure 2E,F). Our analyses of the images taken immediately after the implantation ($t = 0$) indicate that total flux from the implantation sites was directly proportional to the number of cells implanted (Fig 2I). This is consistent with the other data (not shown) demonstrating linear relationship between the light emission and the number of cells plated *in vitro*. Based on these results, we demonstrated that bioluminescence measurement is a plausible method to accomplish non-invasive monitoring of the early tumor growth *in vivo*.

### Detection of a Single Bioluminescent 4T1-luc2 Cell *In Vivo*

After confirming non-invasive detection of three cells *in vivo*, we challenged ourselves to detect a single 4T1-luc2-1A4 cell after subcutaneous implantation. To eliminate the experimental error and to add accuracy to the determination of the number of implanted cells, we used a micropipettor to implant a single 4T1-luc-2-1A4 cell. First, the 4T1-luc2-1A4 cells were trypsinized and plated on a cell culture dish. Next, individual cells were picked up and implanted using a micropipettor into subcutaneous slots made in the flank regions of mice. Mice were divided into two groups: four mice were implanted with single cells, and four other mice were implanted with 10 cells each (Figure S4C,D). Animals were then subjected to bioluminescence imaging immediately after the implantation. In some cases, we were able to detect a single 4T1-luc2-1A4 cell (Figure 3A-C and Figure S4A,B). On each of the three independent, sequential images of the same single cell we registered a total flux ranging from 460 to 528 photons/sec. Line profiling analyses of the registered flux from a single cell revealed a signal to background ratio of 6 to 1, with the signal clearly originating from the implantation site (Figure 3D,E). Therefore,

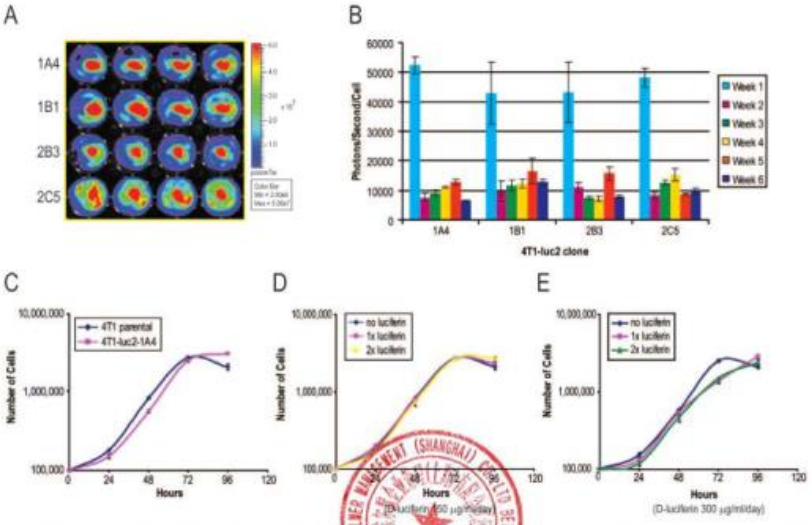


**Figure 1. Generation of 4T1-luc2-1A4 cells and their growth patterns in the presence or absence of D-luciferin.** (A) Generation of 4T1-luc2-1A4 cells. Mouse mammary tumor 4T1 cells were transfected with a lentiviral vector containing enhanced luciferase 2 under control of the human ubiquitin C promoter[16,18]. Puromycin-resistant clones were isolated and their luciferase expressions were screened by bioluminescence. Two rounds of cloning generated 4 single cell clones of 4T1-luc2. Luciferase activities were measured using an IVIS Spectrum (Binning: med, f stop: 1, exposure time: 1 sec). A typical bioluminescence image for testing stability of luciferase expression is shown. Total flux (photons/sec) was quantified using Living Image software 3.0. Clone 4T1-luc2-1A4 was selected and used for further studies. (B) Stability of luciferase activity of four 4T1-luc2 clones. Cells were grown for 6 weeks in regular media without puromycin and their light emission was monitored weekly. All clones showed more than 7,000 photons/sec/cell of light emission throughout the test period. (C) Growth curves of the 4T1-luc2-1A4 clone and parental 4T1 cells. Cells were grown for 4 days in regular growth medium without puromycin. Total numbers of cells over time were plotted in a logarithmic scale. Both cell lines showed similar growth patterns and doubling times. (D,E) Growth of the 4T1-luc2-1A4 clone and parental 4T1 cells in the presence of D-luciferin. Cells were fed with D-luciferin once a day (150 μg/ml/day, D) or twice a day (300 μg/ml/day, E), respectively, harvested at each time point and counted. Presence of the excess of D-luciferin did not affect the overall growth patterns of the 4T1-luc2 cells.
doi:10.1371/journal.pone.0009364.g001

we concluded that the bioluminescent signal indeed originated from a single 4T1-luc2-1A4 cell. The lack of signal from the other three sites in each group could be attributed to rapid cell death.

## Tumor Development from Small Populations of 4T1-luc2 Cells

After detecting a single cell *in vivo*, the mice implanted with 1–50 cells were monitored for extended period of time to detect possible tumor growth. We hypothesized that implantation of larger numbers of cells would circumvent the problem that hostile post-implantation environments present to smaller numbers of cells. Given that routine tumor implantation procedures utilize 0.5 to 10 millions of cells in subcutaneous tumor models, we did not expect tumors to arise from such small numbers of cells. To our surprise, two mice that were implanted with 5 and 10 cells developed solid tumors. We continued to image these mice, and once the tumors became palpable, we also physically measured their dimensions using standard calipers. The tumors arising from 5-cell and 10-cell implantations could not be detected with calipers before day 27 and day 29, respectively (Figure 3G,I). However, non-invasive visible light imaging, allowed us to detect and quantify tumor burdens continuously from the time of implantation (Figure 3F,H). These data clearly show that tumor growth can be monitored using non-invasive bioluminescence imaging as soon as cells are implanted in an animal, even when as few as five cells are implanted.

## Metastases of 4T1-luc2-1A4 Cells in Syngeneic Balb/c Mice from the Orthotopic Implantation into the Mammary Fat Pad

To test metastatic properties of the 4T1-luc2-1A4 cells, we orthotopically implanted these cells into mammary fat pads of female nu/nu mice ($5\times10^5$ cells per mouse, n = 9). The primary tumors grew rapidly and developed metastatic lesions that could be detected using bioluminescence imaging by day 27 (Figure 4). To confirm metastasis of tumor cells into lungs, we isolated lung tissues on day 27 post-implantation and took *ex vivo* images (Figure 4B). In addition, we performed histological analyses on formalin-preserved, paraffin sectioned tissues. The results showed that pleura and subpleural regions of the lungs were infiltrated

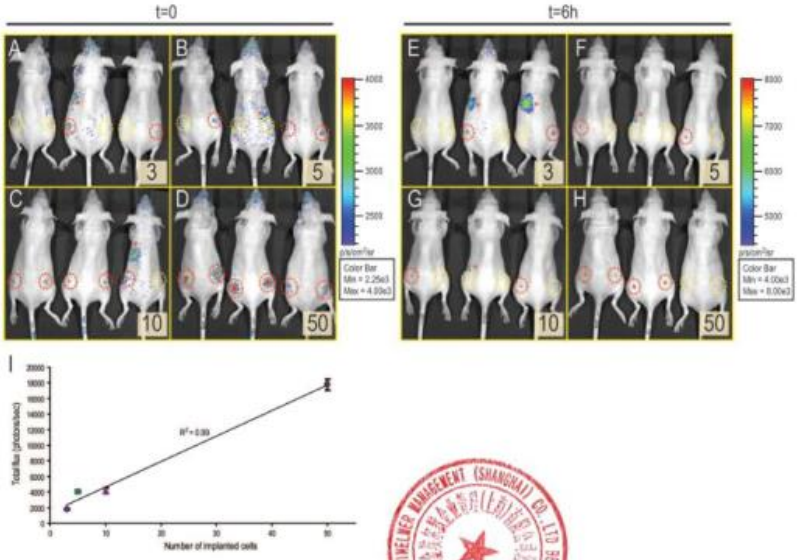


**Figure 2. Detection of small numbers of 4T1-luc2-1A4 cells *in vivo*.** (A–D) Defined numbers of cells were implanted subcutaneously in dorsal flank regions of female nu/nu mice[1]. Each mouse received two implantations. Insets indicate the number of cells implanted. D-luciferin was injected into mice immediately after the implantation and bioluminescent images were taken (t = 0) using the IVIS Spectrum (FOV; A, binning; small, f stop; 1, exposure time; 5 min). (E–H) After 6 hours of implantation, all mice were re-imaged using the same settings of IVIS Spectrum (t = 6h). Red circles represent the implantation sites that had bioluminescent signals higher than autoluminescence. Yellow circles indicate the implantation sites that did not generate any meaningful signals possibly due to immediate cell death. (I) Correlation between the number of implanted cells and the total flux from the implantation sites. Bioluminescent signals were quantitated using Living Image software 3.0 and plotted against the numbers of cells. The measured intensity of bioluminescence was directly proportional to the number of implanted cells. Asterisks (*) indicate tissue autoluminescence.
doi:10.1371/journal.pone.0009364.g002

with sheets of poorly differentiated neoplastic cells demonstrating that bioluminescent imaging can effectively detect micrometastases in a mouse (Figure 4C,D). However, it is difficult to speculate exactly how many cells resided in the metastasized tumor masses based on the light emission registered *in vivo* since the emitted light is attenuated and scattered depending on path it takes through the tissues, and the exact location of these tumors has not been elucidated.

Next, we confirmed the detection of metastases by bioluminescence via physical dissection. We created a second group of Balb/c mice, into whose mammary fat pads we implanted $5.0\times10^4$ 4T1-luc2-1A4 cells (n = 16). Primary tumors were then resected at post-implantation day 10 to stop the growth of the tumors in the fat pads, and bioluminescent images were taken at various post-resection (PR) time points (PR-day 5, 8, 12, 15, 19, 22). Our data showed that tumors metastasized into the secondary sites in the body and continued to grow there (Figure 5A). Tumor growth was monitored longitudinally by quantitating bioluminescence signals from the whole body (Figure 5B). The results demonstrated continuous increase of the light emission before and after resection of the primary tumors, confirming that monitoring bioluminescence signals is an ideal way to track tumor metastases.

## Discussion

Xenografting of luciferase-labeled cancer cells is widely accepted in models of metastasis and in orthotopic models. As discussed above, bioluminescent imaging of luciferase-labeled cancer cells has the added advantage over traditional methods of assessing tumor burden in that it allows non-invasive detection and quantitation of tumors in live animals as means of assessing drug efficacy[21,22,23]. Despite the fact that tissues normally contribute little background in bioluminescence imaging, increasing the light emission from the cells of interest is always desirable since it improves the sensitivity of detecting tumor cells. Increased sensitivity allows smaller numbers of tumor cells present in early stages of tumor progression to be detected. This conceivably has significant clinical relevance given that early detection, when combined with early treatment, has been correlated with better prognoses. The tools described here allow one to compare the effectiveness of a given pharmacological intervention on early stage primary tumors, late stage primary tumors, and metastases.

Herein we report development of a bright 4T1-luc2 cell line using enhanced luciferase (*luc2*) and lentiviral technology. In our

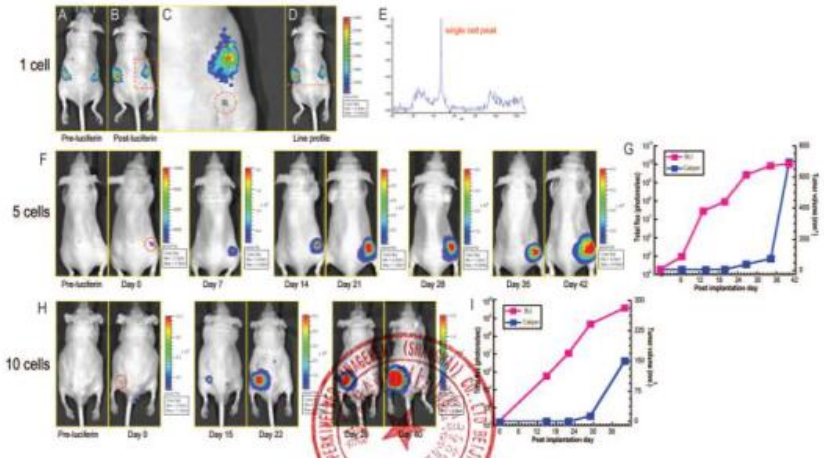


**Figure 3. Detection of a single 4T1-luc2-1A4 cell *in vivo*.** (A-C) Bioluminescent signal of a single 4T1-luc2-1A4 cell *in vivo*. A single cell was implanted into the back of a *nu/nu* mouse. D-luciferin was injected into the mouse intraperitoneally and bioluminescent images were taken using an IVIS Spectrum (FOV; C, binning; small, f stop; 1, exposure time; 5 min). Images for pre- and post-luciferin injection were shown in panels (A) and (B), respectively. Magnified image of the dotted area from panel (B) is shown on panel (C). The dotted circle represents the single cell signal. The asterisk (*) indicates the background signal from the gut. (D,E) Line profiling analysis of single cell signal. Light emission was plotted along the line shown on panel (D). Peak signal in the panel (E) represents the light emission from a single 4T1-luc2-1A4 cell. (F) Tumor development from five 4T1-luc2-1A4 cells. Cells were implanted subcutaneously (using a micropipette) into the dorsal flank region of a *nu/nu* mouse. Bioluminescent images were first taken before the D-luciferin injection (Pre-luciferin). The animal was then imaged on day 0 through day 42. (G) Monitoring of tumor growth from 5 cells of 4T1-luc2-1A4. Bioluminescent signals were quantified using Living Image software and plotted against physical tumor volume measurements by a caliper. Tumor was not palpable till day 27 post-implantation while bioluminescent signals were detected from the day 0. Note that total flux was plotted in a logarithmic scale. (H) Tumor development from 10 cells of 4T1-luc2-1A4. Cells were implanted subcutaneously (using a micropipette) into the back of a *nu/nu* mouse. The background signal is shown in pre-D-luciferin injection image (Pre-luciferin). The tumor growth was monitored for 40 days using an IVIS Spectrum and a caliper. (I) Monitoring of tumor growth from 10 cells of 4T1-luc2-1A4. Tumor volumes were measured using a caliper and plotted against bioluminescent signals which were quantified using Living Image software. Tumor was not palpable till day 29 after implantation. On the contrary, bioluminescent signals were distinct from the day 0 of implantation.
doi:10.1371/journal.pone.0009364.g003

attempts to detect small numbers of cells, we initially used a serial dilution method and could detect down to 3 cells *in vivo*. Encouraged by these results, we challenged ourselves to detect a single 4T1-luc2-1A4 cell after subcutaneous implantation via microinjection. Because the signal from a cell was located in proximity to the gut, which exhibits an intrinsic, albeit variable auto-bioluminescence, our images of single cells contain both, signals from the cell, as well as background from the gut (Figure 3B). However, as shown on the images of 5- and 10-cells, when the numbers of cells increased, the signals from the cells quickly surpassed the background signals from the gut. During the course of preparation of this manuscript, Rabinovich *et al.* showed the detection of three engineered murine T lymphocytes *in vivo* in a subcutaneous transplantation[24]. While application of the elegant system described by Rabinovich *et al.* was developed to achieve efficient transduction for a specific cell subtype, we have engineered a simple, universal vector to transduce various types of proliferating and non-proliferating cells. Moreover, to the best of our knowledge, our report is the first one that shows detection of a single bioluminescent cancer cell *in vivo*.

Because high level of luciferase expression increases the sensitivity of cell detection in live animals, this technology can be directly applied to primary cell and stem cell detection *in vivo*, including cancer stem cells[25,26,27]. The lentivirus technology can conceivably prove useful for labeling stem cells since it can significantly minimize handling and culturing of these cells. Our results showed that as few as 5 and 10 cells can grow and form tumors in the animals. These tumors can be monitored using bioluminescence imaging from the day of implantation. Previously, 4T1 cells were transformed with luciferase and their tumor metastases were visualized using optical imaging[28]. While this study demonstrated non-invasive monitoring of tumor metastases, the present study enables earlier detection of tumor metastases, and allows following the tumor formation process right from the cell implantation (Day 0 vs. 6 weeks). Furthermore, our results suggest that labeling and tracking cancers growing from a single cancer stem cell is feasible. In addition, this technology could also be applied more generally to follow the fate of a single stem cell implanted into an animal. Furthermore, the process of drug screening for either small molecules or biologics which target cancer stem cells can be significantly expedited since bioluminescence allows following growth of tumors *in vivo* weeks before they become palpable.

Brightly luminescent cells also provide a better means of detection of micrometastases in an animal, thus making models of

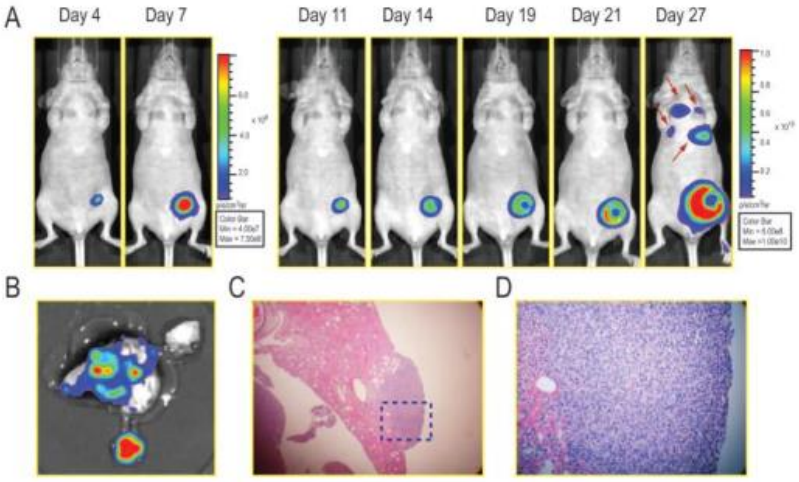


**Figure 4. Non invasive detection of micrometastases and histological analysis.** (A) Female nu/nu mice were inoculated with $5\times10^5$ 4T1-luc2-1A4 cells orthotopically into the abdominal mammary fat pads[1]. Bioluminescent images were taken longitudinally. At post-implantation day 27, micrometastases were detected in lungs (arrows) (B) The lungs were isolated at post-implantation day 27 and *ex vivo* image was taken. (C,D) Lung tissues were fixed in formalin and embedded in paraffin. H&E staining was performed and analyzed. Panel D represents the dotted area in panel C.
doi:10.1371/journal.pone.0009364.g004

metastasis more accurate and allowing predictive models to be tested for evaluation of drug candidates that aim to combat metastases. When 4T1-luc2-1A4 cells were implanted into syngeneic Balb/c mice, we were able to detect multiple micrometastases at secondary sites. When primary tumors were surgically removed at 27 days after the implantation, we could follow the growth of small, metastatic tumors in the absence of the dominating signal from the primary tumor. Brighter cells can reduce the time and effort required to identify tumor masses in an animal and can also be valuable in studying tumor microenvironments, particularly when combined with other non-invasive fluorescence-based readouts.

To date, we have labeled more than a dozen human and murine tumor cell lines using the described lentiviral system (data not shown). All labeled cell lines showed significantly higher luciferase expression compared to the cell lines labeled with previous generation of luciferase and conventional transfection methods (data not shown). Another advantage of these newly engineered cell lines is that no antibiotic selection is required to maintain stable luciferase expression. In contrast to the popular viral promoters such as SV40 or CMV, human ubiquitin C promoter is more resistant to gene silencing in mammalian cells[29]. We have used our technology to successfully label adherent, as well as suspension cell lines, and we believe that it constitutes a universal tool for efficient introduction of luciferase into almost any cell. Since lentiviral vectors can introduce genes of interest into dividing as well as non-dividing cells, our technology can be easily applied to label not only stem cells, but practically any cells derived from patients, which then can be used for research, or for diagnostic purposes.

## Materials and Methods

### Generation of Lentivirus Vector

Enhanced luciferase 2 (*luc2*) cDNA was from pGL4.20 vector (Promega, MI)[16]. Luciferase 2 cDNA was excised with Hind III & Xho I and ligated into pUB6-V5-HisB vector (Invitrogen, CA). A fragment generated by Bgl II and BstB I digestion of pUB6-luc2 was ligated into a modified pLPCX vector (Clontech, CA). A lentiviral vector that carries human ubiquitin C promoter and luc2 cDNA was generated by inserting Bgl II & EcoR I fragment from above construct into Bcl I & EcoR I of the modified pLKO.1 vector (Sigma-Aldrich, MO)[18,19].

### Cell Culture

Mouse mammary gland tumor cell line 4T1 was obtained from the ATCC (Manassas, VA). Cells were grown in high glucose RPMI 1640 medium (ATCC). PC-3M-luc-C6 cells were grown in minimal essential medium (ATCC) (For supplemental data)[30]. All media was supplemented with 10% fetal bovine serum (Hyclone, UT) without antibiotics. Growth curves were generated by seeding 50,000 cells in T25 flasks. At each time point, cells were trypsinized and counted using an automatic cell counter (Nexcelom, MA). Total numbers of cells were plotted in a logarithmic scale.

### Transfection and Stable Cell Line Generation

The lentiviral vector was transfected using a lipid based method into 4T1 cells. Transfected cells were selected using puromycin (2 μg/ml). Isolated clones were screened for their luciferase activities using an IVIS Spectrum (Caliper Life Sciences, MA).

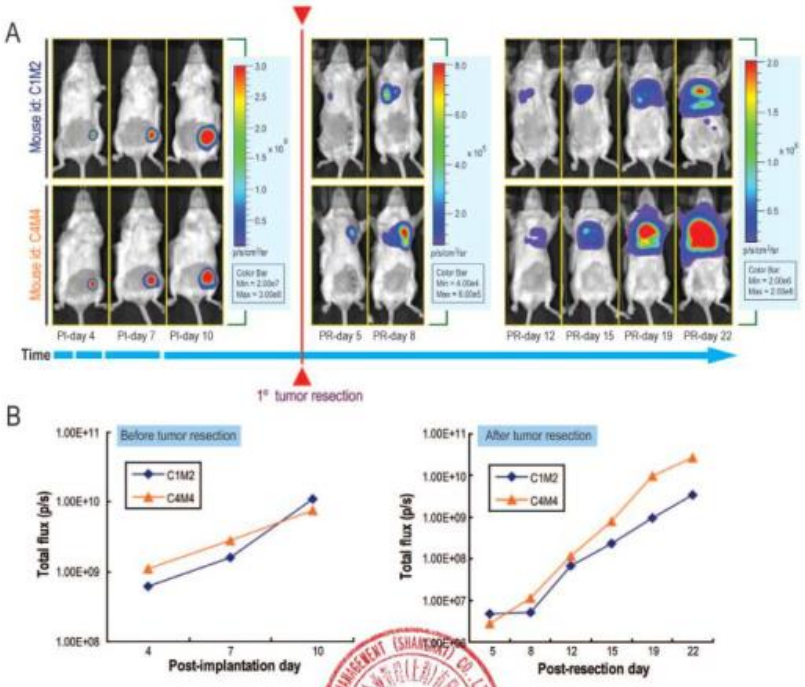


**Figure 5. 4T1-luc2-1A4 tumor metastases in syngeneic Balb/c mice.** (A) Metastases of 4T1-luc2-1A4 tumors in Balb/c mice. $5.0 \times 10^4$ cells were orthotopically implanted into mammary fat pads of the mice (n = 16)[1]. Ventral images were taken at three time points post-implantation (PI-days: 4, 7, 8). Primary tumors were resected at PI-day 10 and images were taken again at various post-resection time points (PR-days: 5, 8, 12, 15, 19, 22). Two representative mice (C1M2 and C4M4) are shown. The apparent decrease of the bioluminescence signals at PR-day 12 was due to the adjustment of the color bar scale (see panel B). Primary tumor resection time point is indicated by the red line separating the pre-and pot-resection images. (B) Plots of bioluminescence signals vs. time for mice C1M2 and C4M4. Whole-body bioluminescence signals of mice C1M2 (blue lines) and C4M4 (orange lines) were quantitated and plotted in a logarithmic scale. Quantitations of bioluminescence signals before and after resection of the primary tumors are shown.
doi:10.1371/journal.pone.0009364.g005

To isolate single cell clones, cells were subjected to limited dilution. Individual clones were screened for luciferase activity using an IVIS® Spectrum. Selected clones were maintained without puromycin for 4 weeks and their light emission was monitored every week.

## Mice and Tumor Cell Implantation

All procedures for animal care and tumor cell implantation followed the approved animal protocols and guidelines of the Institutional Animal Care and Use Committee at Caliper Life Sciences and Momenta Pharmaceuticals. Prior to implantation, all tumor cells tested negative for the presence of mycoplasma and mouse pathogens. The orthotopic implantation of 4T1-luc2-1A4 cells into mammary fat pads of *nu/nu* or Balb/c mice was performed while animals were under isoflurane anesthesia[1]. Subcutaneous implantations were done by injecting cells under the skin in the dorsal flank regions. Single, and ten cell implantation was performed using a customized glass capillary pipette with manual aspiration. After the implantation, pipettes were examined under the microscope to make sure that all cells were implanted. Four implantations were done for each, one and ten cell implantations. For the data shown on Figure 2, six implantations were performed, three mice per each of the two groups.

## *In Vitro* and *In Vivo* Bioluminescence Imaging

For *in vitro* luciferase assay, cells were plated on black walled 24-well plates at an initial concentration of 50,000 cells/well. Cells were grown overnight with regular growth medium. After 24

hours, the regular medium was replaced with the D-luciferin containing medium (150 µg/ml). Bioluminescence images were taken immediately after adding the substrate into the cells using an IVIS Spectrum. Light outputs were quantified using Living Image 3.0 (Caliper Life Sciences, Alameda, CA). Prior to the *in vivo* imaging, the mice were anesthetized with isoflurane. D-luciferin solution was then injected intraperitoneally (150 mg/kg). The mice were imaged using an IVIS Spectrum. Bioluminescent signals were quantified using Living Image 3.0 (Caliper Life Sciences, Alameda, CA).

### Histological Analyses

Female nu/nu mice were inoculated with $5\times10^5$ 4T1-luc2-1A4 cells orthotopically into the abdominal mammary fat pad (n = 9). At day 27 post-implantation, lung tissues were isolated and analyzed histopathologically. Tissues were fixed and embedded in paraffin. H&E staining was performed. Slides were examined by a certified pathologist.

## Supporting Information

**Figure S1** (A) Generation of 4T1-luc2 cells. Mouse mammary tumor 4T1 cells were transfected with a lentiviral vector containing enhanced luciferase 2[18,31]. Puromycin resistant clones were isolated and their luciferase expression was screened by bioluminescence. Initial cloning generated 8 clones of 4T1-luc2. Luciferase activity was measured using an IVIS Spectrum (Binning: med, f stop: 1, exposure time: 1 sec). Total flux (photons/sec) was quantified using Living Image software 3.0. Stability of luciferase activities of the 4T1-luc2 clones were monitored for 4 weeks and their light emission was measured weekly. All clones showed more than 3,000 photons/sec/cell of the light emission throughout the test period. (B) Growth curves of the 4T1-luc2-C27 and the 4T1-luc2-C38 clones vs. parental 4T1 cells. The cells were grown for 4 days in a regular growth medium without puromycin. The total numbers of cells over time are plotted in a logarithmic scale. Both cell lines showed similar growth patterns and doubling times. (C) Growth of the 4T1-luc2-C26 and the 4T1-luc2-C36 clones vs. parental 4T1 cells in the presence of D-luciferin. The cells were fed with D-luciferin once a day (150 µg/ml/day, C) or twice a day (300 µg/ml/day, D), respectively. The cells were harvested at each time point and counted. Presence of excess of D-luciferin did not affect the overall growth patterns of the 4T1-luc2 cells.
Found at: doi:10.1371/journal.pone.0009364.s001 (1.59 MB TIF)

**Figure S2** (A) Limited dilution culture was performed with 4T1-luc2-1A4 cells in four 96-well plates. Cells were grown for 10 days and examined their luciferase expression by adding D-luciferin into the culture media. Bioluminescent images were taken immediately. Wells that did not show any luciferase activity did not contain live cells.
Found at: doi:10.1371/journal.pone.0009364.s002 (5.36 MB TIF)

**Figure S3** (A-D) The 4T1-luc2-C26 and the PC3M-luc-C6 cells were subcutaneously implanted into flank regions of SCID-bg mice. Equal numbers of cells for each cell line was implanted. Bioluminescence images were taken 20 hrs post-implantation using an IVIS Spectrum. Numbers of implanted cells are shown on the inserts. Imaging conditions (A,B; FOV: B, binning: small, f stop: 1, exposure time: 30 sec; C,D; FOV: B, binning: small, f stop: 1, exposure time: 5 min).
Found at: doi:10.1371/journal.pone.0009364.s003 (2.72 MB TIF)

**Figure S4** (A, B) Bioluminescent signal of a single 4T1-luc2-1A4 cell *in vivo*. Female *nu/nu* mouse was implanted with a single 4T1-luc2 cell subcutaneously in the dorsal region. Mouse was imaged prior to D-luciferin injection (A). Ten minutes after the D-luciferin injection, whole mouse image was taken (FOV; C, binning; small, f stop; 1, exposure time; 5 min) (B). Dotted circle indicates the signal from the implanted cell. (C) Whole mouse (*nu/nu*) image with implanted ten 4T1-luc2-1A4 cells. The exact number of cells was picked up by a glass capillary pipet and was injected into the back of the mouse subcutaneously, through a skin incision. (D) Magnified image of dotted area from panel C. Dotted circle indicates the signal from 10 cells. Asterisk (*) indicates the skin incision site.
Found at: doi:10.1371/journal.pone.0009364.s004 (3.57 MB TIF)

## Acknowledgments

The authors thank Drs. Ning Zhang, Victor Ninov, Tamara Troy, Jay Whalen, and Chauncey Kuo for their helpful discussions. The authors also thank Kaling Modi and Minal Tapadia for proofreading the manuscript.

## Author Contributions

Conceived and designed the experiments: JBK. Performed the experiments: JBK KU AA SL EC AB RC AG ZL HZ TKK. Analyzed the data: JBK EC BR HZ TKK PL. Contributed reagents/materials/analysis tools: BR KC RC AG. Wrote the paper: JBK PL.

## References

1. Jenkins DE, Oei Y, Hornig YS, Yu SF, Dusich J, et al. (2003) Bioluminescent imaging (BLI) to improve and refine traditional murine models of tumor growth and metastasis. Clin Exp Metastasis 20: 733–744.
2. Hirsch FR, Franklin WA, Gazdar AF, Bunn PA, Jr. (2001) Early detection of lung cancer: clinical perspectives of recent advances in biology and radiology. Clin Cancer Res 7: 5–22.
3. Holmgren L, O'Reilly MS, Folkman J (1995) Dormancy of micrometastases: balanced proliferation and apoptosis in the presence of angiogenesis suppression. Nat Med 1: 149–153.
4. Killion JJ, Radinsky R, Fidler IJ (1998) Orthotopic models are necessary to predict therapy of transplantable tumors in mice. Cancer Metastasis Rev 17: 279–284.
5. Vaupel P, Kallinowski F, Okunieff P (1989) Blood flow, oxygen and nutrient supply, and metabolic microenvironment of human tumors: a review. Cancer Res 49: 6449–6465.
6. Sommer G, Agosti V, Ehlers I, Rossi F, Corbacioglu S, et al. (2003) Gastrointestinal stromal tumors in a mouse model by targeted mutation of the Kit receptor tyrosine kinase. Proc Natl Acad Sci U S A 100: 6706–6711.
7. Zheng M, Lu R, Che X, Li J, Zhou C, et al. (2006) Tyroservatide therapy for tumor growth, invasion and metastasis of Lewis lung carcinoma and human lung carcinoma A549. Oncology 70: 418–426.
8. Adam M, Bayer C, Henke J, Geoui A, Molls M, et al. (2008) Tirapazamine plus cisplatin and irradiation in a mouse model: improved tumor control at the cost of increased toxicity. J Cancer Res Clin Oncol 134: 137–146.
9. Troy T, Jekic-McMullen D, Sambucetti L, Rice B (2004) Quantitative comparison of the sensitivity of detection of fluorescent and bioluminescent reporters in animal models. Mol Imaging 3: 9–23.
10. Song H, Shahverdi K, Huso DL, Wang Y, Fox JJ, et al. (2008) An immunotolerant HER-2/neu transgenic mouse model of metastatic breast cancer. Clin Cancer Res 14: 6116–6124.
11. Roda A, Guardigli M, Pasini P, Mirasoli M (2003) Bioluminescence and chemiluminescence in drug screening. Anal Bioanal Chem 377: 826–833.
12. Formichova EV, Turner R, Edwards TG, Hall J, Arden E, et al. (2008) Double oxygen-sensing vector system for robust hypoxia/ischemia-regulated gene induction in cardiac muscle in vitro and in vivo. Mol Ther 16: 1594–1601.
13. Cao YA, Wagers AJ, Beilhack A, Dusich J, Bachmann MH, et al. (2004) Shifting foci of hematopoiesis during reconstitution from single stem cells. Proc Natl Acad Sci U S A 101: 221–226.
14. Ray S, Paulmurugan R, Patel MR, Alan BC, Wu L, et al. (2008) Noninvasive imaging of therapeutic gene expression using a bidirectional transcriptional amplification strategy. Mol Ther 16: 1848–1856.
15. Iyer M, Salazar FB, Lewis X, Zhang L, Carey M, et al. (2004) Noninvasive imaging of enhanced prostate-specific gene expression using a two-step transcriptional amplification-based lentivirus vector. Mol Ther 10: 545–552.
16. Promega (2007) pGL4 luciferase reporter vectors. Promega Technical Manual. TM259.

17. Schorpp M, Jager R, Schellander K, Schenkel J, Wagner EF, et al. (1996) The human ubiquitin C promoter directs high ubiquitous expression of transgenes in mice. Nucleic Acids Res 24: 1787–1788.
18. Zufferey R, Nagy D, Mandel RJ, Naldini L, Trono D (1997) Multiply attenuated lentiviral vector achieves efficient gene delivery in vivo. Nat Biotechnol 15: 871–875.
19. Pfeifer A, Kessler T, Silletti S, Cheresh DA, Verma IM (2000) Suppression of angiogenesis by lentiviral delivery of PEX, a noncatalytic fragment of matrix metalloproteinase 2. Proc Natl Acad Sci U S A 97: 12227–12232.
20. Scatena CD, Hepner MA, Oei YA, Dusich JM, Yu SF, et al. (2004) Imaging of bioluminescent LNCaP-luc-M6 tumors: a new animal model for the study of metastatic human prostate cancer. Prostate 59: 292–303.
21. Uhrbom L, Nerio E, Holland EC (2004) Dissecting tumor maintenance requirements using bioluminescence imaging of cell proliferation in a mouse glioma model. Nat Med 10: 1257–1260.
22. Zhang GJ, Safran M, Wei W, Sentman L, Takita J, Chiang AW, et al. (2004) Bioluminescent imaging of Cdk2 inhibition in vivo. Nat Med 10: 643–648.
23. Brakenhielm E, Burton JB, Johnson M, Adams RH, Mamluk R, et al. (2007) Modulating metastasis by a lymphangiogenic switch in prostate cancer. Int J Cancer 121: 2153–2161.
24. Rubinovich BA, Ye Y, Emu T, Chen CJQ, Levinsky DL, et al. (2008) Enabling fewer than 10 mouse T cells with an enhanced firefly luciferase in immunocompetent mouse models of cancer. Proc Natl Acad Sci U S A 105: 14342–14346.
25. Kondo T, Setoguchi T, Taga T (2004) Persistence of a small subpopulation of cancer stem-like cells in the C6 glioma cell line. Proc Natl Acad Sci U S A 101: 781–786.
26. Dylla SJ, Beviglia L, Park IK, Chartier C, Raval J, et al. (2008) Colorectal cancer stem cells are enriched in xenogeneic tumors following chemotherapy. PLoS ONE 3: e2428.
27. Dalerba P, Dylla SJ, Park IK, Liu R, Wang X, et al. (2007) Phenotypic characterization of human colorectal cancer stem cells. Proc Natl Acad Sci U S A 104: 10158–10163.
28. Tao K, Fang M, Alroy J, Sahagian GG (2008) Imagable 4T1 model for the study of late stage breast cancer. BMC Cancer 8: 228.
29. Gill DR, Smyth SE, Goddard CA, Pringle IA, Higgins CF, et al. (2001) Increased persistence of lung gene expression using plasmids containing the ubiquitin C or elongation factor 1alpha promoter. Gene Ther 8: 1539–1546.
30. Kuo C, Coquoz O, Troy TL, Xu H, Rice BW (2007) Three-dimensional reconstruction of in vivo bioluminescent sources based on multispectral imaging. J Biomed Opt 12: 024007.
31. Pfeifer A, Kessler T, Yang M, Baranov E, Kootstra N, et al. (2001) Transduction of liver cells by lentiviral vectors: analysis in living animals by fluorescence imaging. Mol Ther 3: 319–322.

## 21 检测灵敏度证明文献 2

# Visualizing fewer than 10 mouse T cells with an enhanced firefly luciferase in immunocompetent mouse models of cancer

Brian A. Rabinovich*[1], Yang Ye*, Tamara Etto*, Jie Qing Chen*, Hyam I. Levitsky[†], Willem W. Overwijk*, Laurence J. N. Cooper*, Juri Gelovani*, and Patrick Hwu*

*M. D. Anderson Cancer Center, 7455 Fannin Street, Houston, TX 77054; and [†]Johns Hopkins University School of Medicine, Sidney Kimmel Comprehensive Cancer Center, 1650 Orleans Street, Baltimore, MD 21231

Edited by Pamela J. Bjorkman, California Institute of Technology, Pasadena, CA, and approved August 15, 2008 (received for review April 29, 2008)

**Antigen specific T cell migration to sites of infection or cancer is critical for an effective immune response. In mouse models of cancer, the number of lymphocytes reaching the tumor is typically only a few hundred, yet technology capable of imaging these cells using bioluminescence has yet to be achieved. A combination of codon optimization, removal of cryptic splice sites and retroviral modification was used to engineer an enhanced firefly luciferase (ffLuc) vector. Compared with ffLuc, T cells expressing our construct generated >100 times more light, permitting detection of as few as three cells implanted s.c. while maintaining long term coexpression of a reporter gene (Thy1.1). Expression of enhanced ffLuc in mouse T cells permitted the tracking of <3 × 10[4] adoptively transferred T cells infiltrating sites of vaccination and preestablished tumors. Penetration of light through deep tissues, including the liver and spleen, was also observed. Finally, we were able to enumerate infiltrating mouse lymphocytes constituting <0.3% of total tumor cellularity, representing a significant improvement over standard methods of quantitation including flow cytometry.**

bioluminescence | immunology | molecular biology

Complete resolution of infection or cancer often depends on an effective T cell mediated immune response. In many cases, in particular that of a tumor setting, only hundreds of tumor-specific T cells traffic to the tumor. To date, the signal intensity generated by bioluminescent (BLI) reporter genes has been insufficient to track fewer than tens of thousands of T cells in living animals. This has made it very difficult to study strategies for improving tumor homing.

In addition to BLI, positron emission tomography (PET) (1) and intravital microscopy (IVM) (2, 3) offer dynamic imaging but are less applicable to routine preclinical studies because of their expense and laborious nature. PET also requires the use of radioactive substrates and IVM is highly invasive and generally requires that studied animals be euthanized. Recently, IVM was used to image tumor specific T cells at tumor sites indicating that tumor cell killing by an individual T cell occurs slowly (> 6 h) (4).

Pioneered by Contag *et al.* and using bioluminescent bacteria (5), BLI is among the most commonly used modalities for noninvasive imaging of small animals. To date, the luciferase genes from *Photinus* pyralis (American firefly; ffLuc), *Pyrophorus* plagiophthalamus (CB-Luc), *Renilla* reniformis (rLuc), and Gaussia *princes* (gLuc) are the most commonly used light emitting reporters. Of these, only ffLuc and CB-Luc catabolize a substrate (D-Luciferin) that is relatively stable *in vivo*. gLuc and rLuc catabolize coelenterazine but their use is limited by background luminescence (6), rapid clearance of their substrate, and flash kinetics and blue/green emission, respectively (7, 8).

Mouse T cells expressing ffLuc have been obtained from transgenic (tg) mice (9–11), bone marrow (BM) chimeric mice (obtained after lentiviral transduction of donor BM) (12), and direct retroviral transduction of T cells *in vitro* (13, 14). Unfortunately, ffLuc is expressed poorly in mouse T cells resulting in poor sensitivity of detection (at the level of thousands of cells), requiring investigators to acquire images with high binning densities [8–16 pixels (px) grouped together) to capture weak signals in general areas (9, 13–15). In digital imaging, a px is the smallest piece of data in an image. For review, see ref. 16.

Experience from human clinical trials employing the adoptive transfer of expanded autologous tumor-infiltrating T cells into cancer patients indicates that very small numbers of lymphocytes (<0.005% per gram of tumor) reach the tumor (17). To date, most reports studying T cell trafficking to tumors have been performed in xenograft models because expression of ffLuc in human T cells provides sufficient sensitivity for BLI (18–23). These models, however, do not consider the complex interplay of T cells with an autologous immune system. Several investigators have thus attempted to use BLI for T cell trafficking in immunocompetent models of cancer, but because of the weak signal intensity generated by ffLuc-expressing T cells, images had to be acquired using high binning density ($\rho$) ($\approx 256 \times 256$ px) (15, 24). Comparison of xenogeneic and syngeneic systems has been recently performed in a model of mammary carcinoma in which BLI was clearly superior in the xenogeneic system (24). Other models investigating the trafficking of ffLuc-expressing mouse T cells have also necessitated high px $\rho$, thus limiting spatial analysis. These include collagen-induced arthritis (CIA) (14), experimental autoimmune encephalitis (EAE) (13) and graft versus host disease (GVHD) (10, 12, 25).

We engineered an enhanced version of ffLuc (effLuc) encoded within a retroviral vector to facilitate detection of <10,000 T cells at a given site in living animals. Retroviral transduction was chosen because it is a rapid procedure (3 days) for achieving stable expression of a given gene, which facilitates subsequent experimentation within days to weeks. Compared with mouse T cells expressing ffLuc, those expressing effLuc generated >100 times as much detectable light. Further, the augmented signal intensity provided the means to image as few as three effLuc-expressing T cells and to examine the limits of detection of cells expressing effLuc in models of vaccination and adoptive immunotherapy of established tumors.

## Results

**Construction of an Enhanced Firefly Luciferase and Expression in Mouse T Cells.** We made modifications to an ffLuc encoding retroviral vector (pMSCV-ffLuc-pIRES2-Thy1.1 [v-ffLuc]) to

Author contributions: B.A.R., L.J.N.C., and P.H. designed research; B.A.R., Y.Y., J.Q.C., and W.W.O. performed research; B.A.R., Y.Y., T.E., J.Q.C., W.W.O., J.G., and P.H. analyzed data; H.I.L. and L.J.N.C. contributed new reagents/analytic tools; and B.A.R. and T.E. wrote the paper.

The authors declare no conflict of interest.

This article is a PNAS Direct Submission.

[1]To whom correspondence should be addressed. E-mail: brabinov@mdanderson.org.

This article contains supporting information online at www.pnas.org/cgi/content/full/0804105105/DCSupplemental.

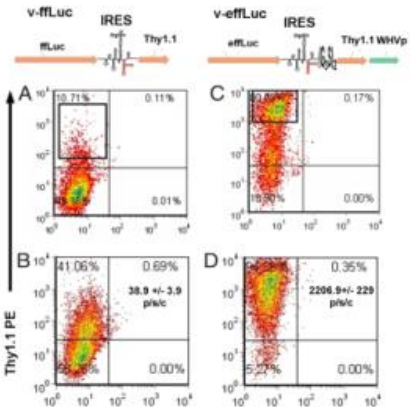


**Fig. 1.** Comparison of coreporter expression and *in vitro* luminescent activity of T cells expressing standard versus enhanced retroviral firefly luciferase constructs. OT.1 T cells were transduced with the retroviruses v-ffLuc (*A* and *B*) or v-effLuc (*C* and *D*) (illustrations of vector coding regions are shown above each column) and assessed for Thy1.1 expression 3 days later via flow cytometry (*A* and *C*). The boxed areas represent the regions chosen for sorting. 7 days after sorting, transduced T cells were reassessed for longevity of Thy1.1 expression. (*B* and *D*) OT.1 T cells ($1 \times 10^5$) transduced with the indicated retroviruses were assessed for bioluminescent activity before sorting and after addition of D-Luciferin. Signal intensity (photons per second per cell) is in the top right quadrant of *B* and *D*.

improve expression of the reporter transgene, in particular for mouse T cells. Thy1.1 was chosen as the coreporter because it differs from its allelic variant Thy1.2 sufficiently to be detected by a specific monoclonal antibody but is not immunogenic in Thy1.2$^+$ strains. Mouse CD8 OT-1 TCR tg T cells specific for Ovalbumin peptide 257–264 in the context of H2-kb (26) transduced with v-ffLuc demonstrated weak Thy1.1 (flow cytometry) and luciferase activity (*in vitro*). (Fig. 1 *A* and *B*). To generate an improved construct, effLuc, we added a $(G_3S)_2$ linker to the 3′ end of the pIRES2 [supporting information (SI) Fig. S1], codons were optimized to the highest frequency of *Mus musculus* and a Woodchuck Hepatitis Virus (WHV) pre element was added downstream of Thy1.1 to augment export of the viral mRNA into the cytosol (27). Construct illustrations are shown in Fig. 1. Codon optimization lead to the modification of three consensus acceptor splice sites (positions 131, 894, and 1004), 9 cryptic acceptor sites (positions 194, 305, 551, 639, 669, 801, 1011, 1112, and 1403) and five cryptic donor sites (positions 334, 349, 1083, 1169, and 1173). One consensus (position 1433) and two cryptic donor splice sites (positions 334 and 1173) from the ffLuc ORF were eliminated by the GeneOptimizer software. Removal of cryptic splice sites was considered important for mouse T cells because excessive aberrant splicing has been reported as a protective tactic used by mouse T cells against retroviral infection (28).

These modifications resulted in >80% of effLuc-transduced T cells expressing Thy1.1 (a 6-fold increase) and a >100-fold increase in Thy1.1 mean fluorescent intensity in the unsorted population. Less than 25% of effLuc OT-I lost Thy1.1 expression over 7 days of culture compared with >85% for ffLuc. During this time, relative to ffLuc-expressing T cells, luciferase acitivity from effLuc-expressing OT-I T cells increased from 60% to >250% (Fig. S2*B*). After sorting, we found that effLuc-transduced (compared with ffLuc-transduced) T cells demonstrated a >55-fold increase in intensity [photon flux (the radiance (cm$^2$) $\times$ $4\pi$ at a given cell number]. The signal intensity of OT-I effLuc versus OT-1 ffLuc was 2,206.9 $\pm$ 229 photons per second per cell and 38.9 $\pm$ 3.9 photons per second per cell, respectively (Fig. 1 *B* and *D*). We also observed a 100- to 110-fold increase in sensitivity (number of cells detected at the same photon flux) (Table S1). Viral integration, measured on days 3 and 5 after transduction, was 4- to 6-fold better for v-effLuc versus v-ffLuc (Fig. S3), thus the increase in luciferase acitivity is a function of both integration efficiency and expression efficiency.

Because the levels of firefly luciferase expression reported here are superior to previously observed, we compared several parameters of *in vitro* immunological function between sorted v-ffLuc, v-effLuc, and untransduced OT-I cells. We found no differences in proliferation, cytotoxicity, or IFN-$\gamma$ production (Fig. S4). Interestingly, in the unsorted population, we found that, at 24 h after transduction, the number of cells in the v-ffLuc population was approximately half that in the v-effLuc. The proliferation curves normalized after 24 h (Fig. S5). Because there was no difference in cell viability, we speculate that the initial difference was due to diminished proliferation of ffLuc OT-I cells that were forced to handle the expression of ffLuc, which utilizes many rare codons.

effLuc was designed for mouse T cells. Nevertheless, we hypothesized that effLuc should provide enhanced sensitivity when transduced into a variety of tissues. We transduced a panel of human and mouse cell lines to investigate the universal applicability of this technology. We found that enhanced intensity and sensitivity of effLuc versus ffLuc ranged from 10- to 250-fold and 40- to >400-fold, respectively (Table S1).

**Imaging effLuc-Expressing T Cells *in Vivo*.** C57BL/6 T cells were transduced with each of the two constructs, and T cell numbers ranging from 3 to 30,000 were injected s.c. into C57BL/6 (B6) Albino mice. The limit of detection for T cells transduced with ffLuc was between 10,000 and 30,000 cells. We found that <300 T cells expressing effLuc were required to match the photon flux of 30,000 T cells expressing ffLuc ($2.7 \times 10^5 \pm 1.3 \times 10^4$ versus $8 \times 10^4 \pm 8.3 \times 10^3$ photons/sec/ROI). Thus, effLuc resulted in an increase in sensitivity of 200–400 times (Fig. 2*A*). Strikingly, we found that as few as three T cells expressing effLuc could be imaged even when acquisition was performed using a binning setting of 4 ($512 \times 512$ px) (Fig. 2*B*). These results suggest that effLuc should permit the study of detailed trafficking patterns of even small populations of lymphocytes. Moreover, although there was 40% loss in signal, ≤300 effLuc-expressing T cells could still be detected through the pigmented skin of wild type C57BL/6 mice. This will allow for imaging studies in a wide variety of tg and knockout animals not available on albino strains (Fig. S6).

Our *in vivo* images of effLuc T cells were acquired using a small px $\rho$ (binning of 4), allowing us to pinpoint T cell location with better confidence than has been historically possible with ffLuc T cells, which requires larger px $\rho$ settings (binning of 8–16 corresponding to $256 \times 256$ and $128 \times 128$ px, respectively) to raise the signal above the noise (9, 13, 14).

We examined the difference in sensitivity between T cells transduced with v-ffLuc versus v-effLuc in two different immunocompetent animal models. The first was a model of vaccination whereby T cells migrate into the s.c. tissue of the vaccine site. Ova peptide-pulsed or DCs ($10^5$ cells) were injected s.c. into the left or right inguinal region, respectively. On the same day, ffLuc- or effLuc-expressing OT-I T cells ranging from $3 \times 10^4$ to $10^6$ in

APPLIED BIOLOGICAL SCIENCES

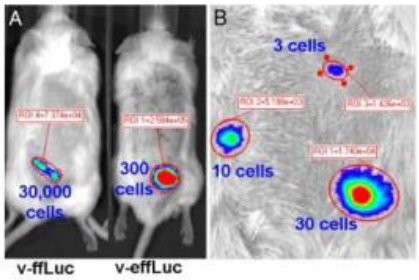


**Fig. 2.** *In vivo* imaging of s.c. implanted T cells transduced with optimized firefly luciferase. (*A*) B6 T cells transduced with v-ffLuc or v-effLuc (as indicated) were injected s.c. at the indicated numbers into B6 Albino mice, and photon emissions were measured on an IVIS 200. (*B*) T cells transduced with v-effLuc were injected s.c. at the level of 30, 10, or 3 cells as indicated.

number, were injected retro-orbitally. Imaging was performed on days 1–6. For both groups, we found that T cells were detected at the site of the Ova vaccination but not the mock vaccination. Results were highly reproducible between animals even when as few as $3 \times 10^4$ T cells expressing effLuc were transferred (Fig. 3*A*). The number of adoptively transferred T cells required for detection at the vaccination site for ffLuc and effLuc was $10^5$ and $\leq 3 \times 10^4$ T cells, respectively. We found that light emission at the vaccination site was ~3-fold higher for animals that received $3 \times 10^4$ versus $10^6$ ffLuc T cells. A representative day 5 image is shown in Fig. 3*B*. This result was highly reproducible at all of the imaging time points. A side by side comparison of luminescent activity of equal numbers of transferred ffLuc- versus effLuc-expressing T cells that migrated to the vaccination site indicated a >100-fold difference in sensitivity, similar to our *in vitro* data (Fig. 3*C*; day 5 is shown). Photon flux produced by T cells transduced with v-effLuc and injected s.c. into the ventral skin of a mouse ($n = 3$), was used to establish a standard curve (Fig. S7) to back-calculate the approximate number of effLuc-expressing T cells in the s.c. tissue in the group receiving $3 \times 10^4$ T cells. This approach indicated that ≤450 T cells had migrated to the vaccination site. Bioluminescence was also observed emanating from deeper tissues (Fig. 3*D*; $10^5$ transferred T cells are shown), which allowed us to perform simple kinetic analysis (Fig. 4*D*). These images capture the trafficking of as few as 0.003% ($3 \times 10^4$ T cells) of the total lymphocyte pool (~$10^9$ cells).

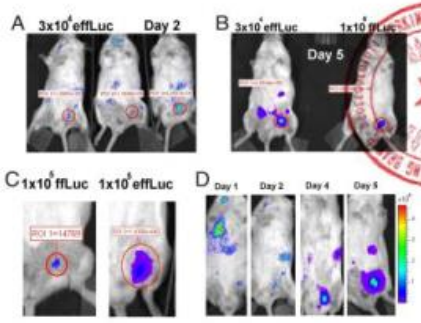


**Fig. 3.** Comparison of migration of OT.1 T cells transduced with v-ffLuc versus v-effLuc to Ova peptide-pulsed DCs. $1 \times 10^6$ Ova-peptide-pulsed or unpulsed dendritic cells were injected into the left or right inguinal region, respectively. Simultaneously, T cells transduced with v-effLuc or v-ffLuc were injected intravenously. (*A*) Mice receiving $3 \times 10^4$ v-effLuc-transduced T cells on day 2. (*B*) Comparison of mice receiving $3 \times 10^4$ v-effLuc-transduced T cells (*Left*) versus $1 \times 10^6$ v-ffLuc-transduced T cells (*Right*), imaged on day 5. (*C*) Comparison of mice that received $1 \times 10^5$ v-ffLuc-transduced T cells (*Left*) versus $1 \times 10^5$ v-effLuc-transduced T cells (*Right*) imaged on day 5. (*D*) Sequential imaging on days 1–6 (days 1, 2, 4, and 5 are shown) of an animal that received $1 \times 10^5$ v-effLuc-transduced T cells. The *y* axis represents photons per second per square centimeter per sr. In each case, a representative experiment is shown.

**Imaging Mouse T Cells in an Established Immunocompetent Tumor Model.** Finally, we evaluated our ability to image effLuc T cells within large preestablished tumors (area >50 $mm^2$) in a well established model of adoptive immunotherapy. B6 Albino mice bearing EL4 (left flank) and Ova-expressing EL4 (EG.7; right flank) tumors were injected retro-orbitally with effLuc-transduced OT-1 T cells ranging in number from $3 \times 10^4$ to $10^6$. The preferential therapeutic efficacy against EG.7 tumors is well described in this model after the transfer of $\geq 3 \times 10^5$ OT.1 T cells (29), a result we duplicated (data not shown). T cells were detected at the site of EG.7 but not EL4 tumors after the transfer of as few as $3 \times 10^4$ T cells (Fig. 4*A*; day 5 is shown). Bioluminescent intensity correlated with the number of transferred T cells (Fig. 4*B*). The observed photon flux at the EG.7 tumor site was used to calculate the number of infiltrating T cells. We investigated whether the photon flux of effLuc T cells injected intratumorally (IT) was lower than those injected s.c.. No statistically significant difference was observed (Fig. S8). Consequently, even when $10^6$ OT.1 T cells were transferred, our calculations estimate an infiltrate on day 5 of only $3–5 \times 10^3$ cells. We excised the tumors and subjected them to Thy1.1 detection by flow cytometry (Fig. 4 *C* and *D*) or IHC (Fig. 4 *E–H*). We found that Thy1.1$^+$ cells were observed at a frequency of <0.3%. In our opinion, flow cytometry cannot accurately quantitate cell numbers at these levels. Using IHC, the number of positive cells varied widely between tissue sections. This indicates that BLI of mouse T cells expressing effLuc is a more accurate method of cell number quantitation and subject to less handling error, variation, and human interpretation.

## Discussion

In this report we addressed the long-standing problem of how to express ffLuc in mouse T cells at sufficient magnitude to achieve a signal intensity suitable to detect <10,000 T cells at a given location and track ≤0.003% of the lymphoid pool within living mice. We decided to focus on retroviral vectors and transduction because this procedure is rapid, simple, and less expensive than crossing ffLuc-tg mice onto immunologically relevant backgrounds.

We made several changes to the standard retro-viral construct encoding (1) ffLuc, (2), an EMCV IRES and (3) Thy1.1. We added a $(G_4S)_2$ flexible linker at the 3′ end of the IRES to facilitate wild type RNA folding (RE-IRES). Next, we proceeded to codon optimize, remove cryptic splice sites from ffLuc and add a WHV pre element. These modifications resulted in >100-fold increase in luciferase activity and Thy1.1 expression intensity. Our data indicate that tRNA availability and cryptic splicing are the major factors limiting expression of ffLuc in mouse T cells after transduction. We found that, compared with ffLuc, transduction of effLuc into human PBMC-derived T cells resulted in only a 10-fold increase in light emission (Table S1).

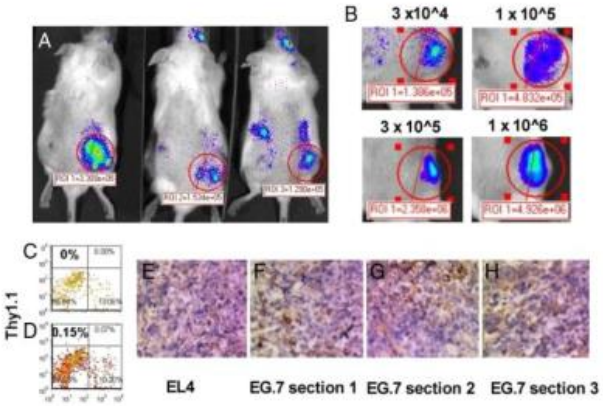


**Fig. 4.** Small numbers of adoptively transferred tumor specific T cells can be detected at preexisting tumors. B6 Albino mice were sublethally irradiated (300 cGy) and implanted s.c. with $1 \times 10^6$ Ova-expressing EL4 (EG.7) tumor cells in the right flank. The same number of control EL4 cells was implanted on the left flank. Seven days later, different numbers of OT.1 T cells transduced with v-effLuc were intravenously injected into the animals. Five days after adoptive transfer, animals were imaged. (*A*) A group of animals injected with $3 \times 10^4$ OT.1 T cells. (*B*) A representative example of tumor infiltration on day 5 after transfer of effLuc-expressing OT.1 T cells (as indicated). (*C–G*) EL4 (*C* and *E*) and EG.7 (*D*, *F*, and *G*) tumors were resected 5 days after adoptive transfer of $1 \times 10^6$ effLuc-expressing OT-I T cell and examined for Thy1.1 expression by either flow cytometry (*C* and *D*) or immunohistochemistry (*E* and *F*).

This interspecies difference in ffLuc expression is important because it has allowed for the study of T cell trafficking to solid tumors in xenogeneic models and validation of the therapeutic efficacy of chimeric activation receptors (18–23). Such models, however, are difficult to evaluate from a dynamic immunological perspective because they necessitate the use of immunodeficient mice.

Our data suggest that the use of effLuc will provide sufficient sensitivity to investigate differences in trafficking and efficacy between different populations of only $3–10 \times 10^4$ adoptively transferred, phenotypically distinct, or genetically modified, tumor-specific T cells (0.003–0.005% of the lymphoid pool). Using a standard curve of effLuc-expressing T cells injected s.c. or IT, we were able to back calculate the approximate number of T cells at a s.c. or IT site. Although three replicate mice were used to establish these curves for each experiment, we feel that the calculated T cell numbers should be considered semiquantitative. Further, compared with s.c., IT injection resulted in what appeared to be a trend toward a 25% loss in signal, but we could not establish statistical significance. Current adoptive immunotherapeutic regimens involve the transfer between 1 and 40 billion heterogeneous tumor specific T cells. In the setting of metastatic melanoma, tumor infiltration has been measured as <0.005% per gram of tumor (17, 30–32) and therapeutic activity is not predictable (33, 34). The injection of large cell numbers has many drawbacks. The procedure is expensive and labor intensive, results in the transfer of later passage cells that are likely less potent effectors and is complicated by T cell trapping in the lungs that can cause respiratory distress (35) and vascular leak syndrome (36). The use of effLuc in models of adoptive immunotherapy will hopefully provide the technology necessary to resolve these side effects and allow the identification of a small subset(s) of T cells, which are responsible for anti-tumor activity.

In summary, we have developed an optimized version of ffLuc that can be transduced into primary mouse T cells. As few as three T cells expressing effLuc injected s.c., can be imaged in living mice. Our data suggests that this technology is better suited for quantification of ≤0.3% of a population of cells compared with flow cytometry and eliminates variation introduced by tissue disruption. IHC appeared to visualize small cell numbers, but considerable variation was observed between sections at different tissue depths. Crossing ffLuc-tg mice onto the multiple strains currently used as models for studying T cells is a valuable technique for various applications including the response of undisturbed populations to multiple stimuli. It will be interesting to see whether tg mice expressing effLuc will result in superior detection of transgene-expressing cell populations versus ffLuc tg mice. The approach described here offers investigators the ability to address questions more quickly than with tg models. From a therapeutic perspective, it should now be possible to visualize and identify subsets of lymphocytes constituting ≤0.003% of the lymphoid pool that are responsible for different aspects of anti-tumor activity and autoimmunity.

APPLIED BIOLOGICAL SCIENCES

## Methods

**Animals.** C57BL/6J-Tyr-2J/J Albino mice were purchased from The Jackson Laboratory. C57BL/6 OT-I TCR tg mice were bred in the vivarium at M. D. Anderson Cancer Center. The M. D. Anderson Cancer Center Animal Care and Use Committee approved all protocols.

**Construction of Retroviral Vector Encoding Optimized Firefly Luciferase and Thy1.1.** Plasmids were derived from the pMSCV-ffFLuc-pIRES-Thy1.1 encoding ffLuc (pGL3; Promega), EMCV pIRES2 (Clontech) and Thy1.1 (H.I.L., unpublished data). The reengineered EMCV IRES (RE-IRES) includes a 3′ linker $(G_3S)_2$ synthesized by Genscript and cloned between HpaI and *Xho-I* sites. Codon optimization, removal of cryptic splice sites and negative *cis*-acting motifs were performed using GeneOptimizer and synthesized by GeneArt. effLuc was cloned between *Bgl-II* and *Hpa-I* sites. The optimized construct was generated by cloning a *Sal-I* and *Cla-I* flanked WHVpre element (generated via PCR) downstream of Thy1.1 between *Sal-I* and *Cla-I*. All constructs were sequence verified.

**Packaging of Retrovirus.** Retroviral vectors were packaged into ecotropic virus as described in ref. 37 with the noted addition of pCLEco (38) (Addgene) to the transfection mix. Supernatants were concentrated between 25× and 100×, using Centricon Plus-20 Centrifugal Filter Units (Millipore), and then titered on NIH 3T3 cells.

**Transduction of Mouse T Cells.** Splenocytes from C57BL/6 wild type mice or OT-I TCR tg mice were cultured in X-Vivo-15 (Lonza), Normocin (Invivogen), 200 IU Proleukin (Chiron), and 0.1 $\mu$g/ml anti-mouse CD3 (clone 2C11; BD Biosciences). After 22–24 h, retrovirus was added at an MOI of 5 in the presence of polybrene (Sigma) and Lipofectamine 2000 (Invitrogen) at 1.6 $\mu$g/ml and 2 $\mu$g/ml, respectively, and spinfected at 850 × g for 2 h. The following day, cells were washed and expanded in Alpha-MEM, 10% FBS, Normocin, and 200 IU/ml Proleukin. Cells were stained three days after transduction with anti-mouse Thy1.1 PE (BD-PharMingen) and sorted using a FACSVantage (BD Biosciences).

***In Vitro* Bioluminescence Assay.** Transduced T cells were washed in PBS and $1 \times 10^5$ cells tested for light emission in a 96-well format in triplicate in 200 $\mu$l OPTI-MEM/150 $\mu$g/ml D-Luciferin (Xenogen), using a Topcount apparatus (Perkin–Elmer).

**Ova Vaccination Model.** To generate CD11b$^+$ DCs, Bone marrow was harvested from C57BL/6 wild type mice and seeded in 6-well plates at $1 \times 10^6$/ml (5 ml) in Alpha-MEM, 10% FBS, Normocin, and 200 $\mu$g/ml Flt3-L and cultured at 37°C in 7.5% $CO_2$. On day 8, GM-CSF was added to 20 $\mu$g/ml. On day 10, LPS was added at to 100 ng/ml. On day 11, DCs were pulsed with 1 $\mu$g/ml Ova peptide 257–264 (Ovap) and washed, and $1 \times 10^6$ cells were injected into the left inguinal region of C57BL/6 Albino mice. The same number of nonpulsed DCs was injected on the right side. Immediately after DCs injection, $3 \times 10^4 - 1 \times 10^6$ OT-I TCR tg T cells expressing ffLuc or effLuc were injected i.v. via retro-orbital injection. Imaging was performed on days 1, 2, 4, and 5.

**Model of Adoptive Immunotherapy for Cancer.** EL4 or EG.7 tumor cells ($2 \times 10^6$) were injected into the left and right flank of C57BL/6 Albino mice. Seven days later, $3 \times 10^4 - 10^6$ OT-I TCR tg T cells expressing effLuc were injected IV via retro-orbital injection. Imaging was performed on days 4 and 5. In some cases, tumors were resected and examined for Thy1.1 expression either via standard IHC of formalin fixed paraffin embedded sections or via flow cytometry.

***In Vivo* Bioluminescence Imaging.** Isofluorane-anesthetized animals were imaged using an IVIS 200 system (Xenogen) 8 min after i.p. injection of 2 mg of D-luciferin according to the manufacturer's specifications. Living image software was used to analyze the data.

**ACKNOWLEDGMENTS.** The authors thank Sunny D. Armstrong for supporting this work and Will Hauser for his assistance with Living Image 3.0. This work was supported by National Institutes of Health Grants RO1 CA116206, CA120956, and R21 CA129390; M. D. Anderson Cancer Center Grant CA16672; Netherlands Organisation for Scientific Research Veni Grant 916.046.014, and M. D. Anderson Cancer Center Specialized Programs of Research Excellence Grant P50 CA093459.

1. Hardy J, *et al.* (2001) Bioluminescence imaging of lymphocyte trafficking in vivo. *Exp Hematol* 29:1353–1360.
2. Sumen C, Mempel TR, Mazo IBvon Andrian UH (2004) Intravital microscopy: visualizing immunity in context. *Immunity* 21:315–329.
3. Jain RK, Munn LLFukumura D (2002) Dissecting tumour pathophysiology using intravital microscopy. *Nat Rev Cancer* 2:266–276.
4. Breart B, Lemaitre F, Celli SBousso P (2008) Two-photon imaging of intratumoral CD8$^+$ T cell cytotoxic activity during adoptive T cell therapy in mice. *J Clin Invest* 118:1390–1397.
5. Contag CH, *et al.* (1995) Photonic detection of bacterial pathogens in living hosts. *Mol Microbiol* 18:593–603.
6. Otto-Duessel M, *et al.* (2006) In vivo testing of Renilla luciferase substrate analogs in an orthotopic murine model of human glioblastoma. *Mol Imaging* 5:57–64.
7. Zhao H, *et al.* (2005) Emission spectra of bioluminescent reporters and interaction with mammalian tissue determine the sensitivity of detection in vivo. *J Biomed Opt* 10:41210.
8. Tannous BA, Kim DE, Fernandez JL, Weissleder Rbreakefield XO (2005) Codon-optimized Gaussia luciferase cDNA for mammalian gene expression in culture and in vivo. *Mol Ther* 11:435–443.
9. Azadniv M, Dugger K, Bowers WJ, Weaver CCrispe IN (2007) Imaging CD8$^+$ T cell dynamics in vivo using a transgenic luciferase reporter. *Int Immunol* 19:1165–1173.
10. Beilhack A, *et al.* (2005) In vivo analyses of early events in acute graft-versus-host disease reveal sequential infiltration of T-cell subsets. *Blood* 106:1113–1122.
11. Tanaka M, *et al.* (2005) In vivo visualization of cardiac allograft rejection and trafficking passenger leukocytes using bioluminescence imaging. *Circulation* 112:I105–I110.
12. Edinger M, *et al.* (2003) CD4+CD25+ regulatory T cells preserve graft-versus-tumor activity while inhibiting graft-versus-host disease after bone marrow transplantation. *Nat Med* 9:1144–1150.
13. Costa GL, *et al.* (2001) Adoptive immunotherapy of experimental autoimmune encephalomyelitis via T cell delivery of the IL-12 p40 subunit. *J Immunol* 167:2379–2387.
14. Nakajima A, *et al.* (2001) Antigen-specific T cell-mediated gene therapy in collagen-induced arthritis. *J Clin Invest* 107:1293–1301.
15. Kim D, Hung CFWu TC (2007) Monitoring the trafficking of adoptively transferred antigen- specific CD8-positive T cells in vivo, using noninvasive luminescence imaging. *Hum Gene Ther* 18:575–588.
16. Graph RF (1999) *Modern Dictionary of Electronics* (Elsevier Science & Technology, Burlington, MA).
17. Pockaj BA, *et al.* (1994) Localization of 111indium-labeled tumor infiltrating lymphocytes to tumor in patients receiving adoptive immunotherapy. Augmentation with cyclophosphamide and correlation with response. *Cancer* 73:1731–1737.
18. Kowolik CM, *et al.* (2006) CD28 costimulation provided through a CD19-specific chimeric antigen receptor enhances in vivo persistence and antitumor efficacy of adoptively transferred T cells. *Cancer Res* 66:10995–11004.
19. Vera J, *et al.* (2006) T lymphocytes redirected against the κ light chain of human immunoglobulin efficiently kill mature B lymphocyte-derived malignant cells. *Blood* 108:3890–3897.
20. Savoldo B, *et al.* (2007) Epstein Barr virus specific cytotoxic T lymphocytes expressing the anti-CD30ζ artificial chimeric T-cell receptor for immunotherapy of Hodgkin disease. *Blood* 110:2620–2630.
21. Chamoti C, *et al.* (2007) Co-expression of cytokine and suicide genes to enhance the activity and safety of tumor-specific cytotoxic T lymphocytes. *Blood* 110:2793–2801.
22. Brown CE, *et al.* (2007) Tumor-derived chemokine MCP-1/CCL2 is sufficient for mediating tumor tropism of adoptively transferred T cells. *J Immunol* 179:3332–3341.
23. Singh RK, *et al.* (2007) Combining adoptive cellular and immunocytokine therapies to improve treatment of B-lineage malignancy. *Cancer Res* 67:2872–2880.
24. Shankaran V, Ikegrin RSContag CH (2006) Synergistic antitumor effects of immune cytokine and adoptive cell therapy. *Science* 311:1780–1784.
25. Zelenay S, *et al.* (2006) Inhibition of CD4+CD25+ regulatory T-cell function by calmodulin-dependent interleukin-2 production. *Blood* 108:390–399.
26. Hogquist KA, *et al.* (1994) T cell receptor antagonist peptides induce positive selection. *Cell* 76:17–27.
27. Zufferey R, Donello JE, Trono DHope TJ (1999) Woodchuck hepatitis virus posttranscriptional regulatory element enhances expression of transgenes delivered by retroviral vectors. *J Virol* 73:2886–2892.
28. Baumann JG, *et al.* (2004) Murine T cells potently restrict human immunodeficiency virus infection. *J Virol* 78:12537–12547.
29. Helmich BKDutton RW (2001) The role of adoptively transferred CD8 T cells and host cells in the control of the growth of the EG7 thymoma: Factors that determine the relative effectiveness and homing properties of Tc1 and Tc2 effectors. *J Immunol* 166:6500–6508.
30. Economou JS, *et al.* (1996) In vivo trafficking of adoptively transferred interleukin-2 expanded tumor-infiltrating lymphocytes and peripheral blood lymphocytes. Results of a double gene marking trial. *J Clin Invest* 97:515–521.
31. Goedegebuure PS, *et al.* (1995) Adoptive immunotherapy with tumor-infiltrating lymphocytes and interleukin-2 in patients with metastatic malignant melanoma and renal cell carcinoma: A pilot study. *J Clin Oncol* 13:1939–1949.
32. Griffith KD, *et al.* (1989) In vivo distribution of adoptively transferred indium-111-labeled tumor infiltrating lymphocytes and peripheral blood lymphocytes in patients with metastatic melanoma. *J Natl Cancer Inst* 81:1709–1717.
33. Mackensen A, *et al.* (2006) Phase I study of adoptive T-cell therapy using antigen-specific CD8$^+$ T cells for the treatment of patients with metastatic melanoma. *J Clin Oncol* 24:5060–5069.
34. Rosenberg SADudley ME (2004) Cancer regression in patients with metastatic melanoma after the transfer of autologous antitumor lymphocytes. *Proc Natl Acad Sci USA* 101:14639–14645.
35. Glauser FL, *et al.* (1988) Cardiopulmonary toxicity of adoptive immunotherapy. *Am J Med Sci* 296:406–412.
36. Bechard DE, *et al.* (1989) Nonspecific cytotoxicity of recombinant interleukin-2 activated lymphocytes. *Am J Med Sci* 298:28–33.
37. Rabinovich BA, *et al.* (2003) Activated, but not resting, T cells can be recognized and killed by syngeneic NK cells. *J Immunol* 170:3572–3576.
38. Naviaux RK, Costanzi E, Haas MVerma IM (1996) The pCL vector system: Rapid production of helper-free, high-titer, recombinant retroviruses. *J Virol* 70:5701–5705.

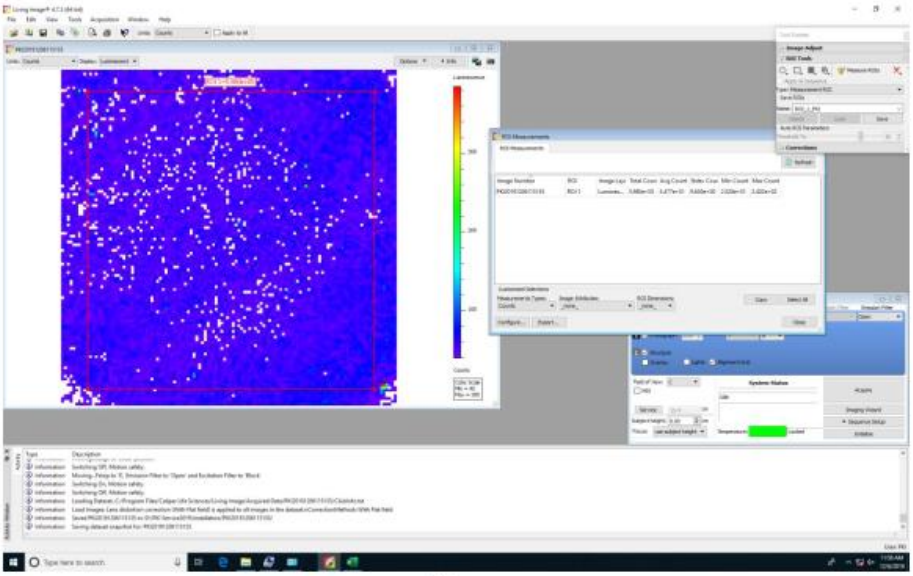

图 34

22. 测试内容：系统的整个感光性一致。

实际测试结果：如图 34 所示，系统经过 NIST 绝对校准，保证系统的整个感光性一致。测试结果符合参数性能指标要求，满足实验需求。

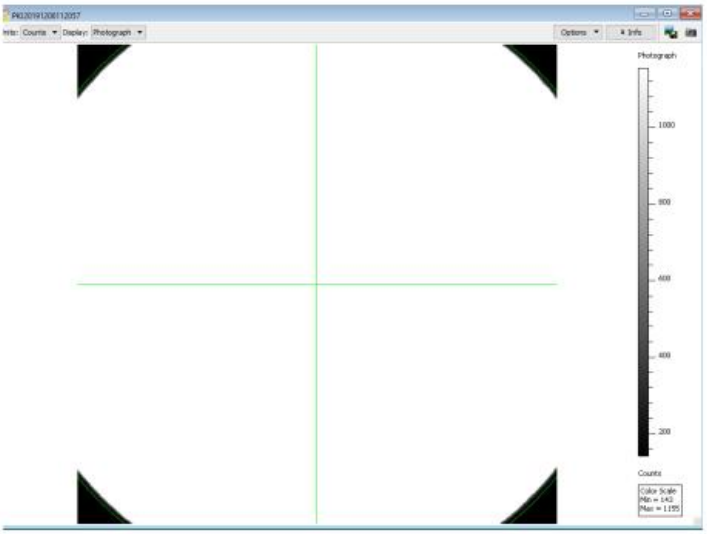


图 35

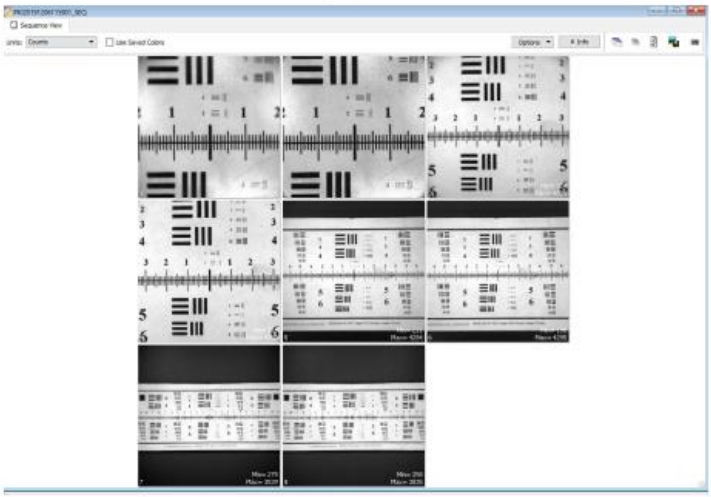


图 36

| Click Number | EX Filter | EM Filter | Illumination Mode | User ID | Group | Experiment | Date and Time | Binning | Exposure | Field of View | f-Stop |
|---|---|---|---|---|---|---|---|---|---|---|---|
| PK20191029161506_001 | 430 | ND3 | Reflective | PKI | Calibration | FL reference images FOV B | 10/30/2019 04:15:23 | 8 | 2 | 6.6 | 2 |
| PK20191029161506_002 | 430 | ND3 | Reflective | PKI | Calibration | FL reference images FOV B | 10/30/2019 04:15:36 | 8 | 12 | 6.6 | 1 |
| PK20191029161506_003 | 465 | ND3 | Reflective | PKI | Calibration | FL reference images FOV B | 10/30/2019 04:15:59 | 8 | 1 | 6.6 | 4 |
| PK20191029161506_004 | 485 | ND3 | Reflective | PKI | Calibration | FL reference images FOV B | 10/30/2019 04:16:10 | 16 | 4 | 6.6 | 4 |
| PK20191029161506_005 | 500 | ND3 | Reflective | PKI | Calibration | FL reference images FOV B | 10/30/2019 04:16:23 | 8 | 4 | 6.6 | 8 |
| PK20191029161506_006 | 500 | ND3 | Reflective | PKI | Calibration | FL reference images FOV B | 10/30/2019 04:16:37 | 16 | 3 | 6.6 | 4 |
| PK20191029161506_007 | 535 | ND3 | Reflective | PKI | Calibration | FL reference images FOV B | 10/30/2019 04:16:49 | 8 | 1 | 6.6 | 8 |
| PK20191029161506_008 | 525 | ND3 | Reflective | PKI | Calibration | FL reference images FOV B | 10/30/2019 04:17:01 | 8 | 1 | 6.6 | 2 |
| PK20191029161506_009 | 570 | ND3 | Reflective | PKI | Calibration | FL reference images FOV B | 10/30/2019 04:17:13 | 8 | 1 | 6.6 | 8 |
| PK20191029161506_010 | 570 | ND3 | Reflective | PKI | Calibration | FL reference images FOV B | 10/30/2019 04:17:24 | 8 | 3 | 6.6 | 4 |
| PK20191029161506_011 | 605 | ND3 | Reflective | PKI | Calibration | FL reference images FOV B | 10/30/2019 04:17:38 | 8 | 1 | 6.6 | 8 |
| PK20191029161506_012 | 605 | ND3 | Reflective | PKI | Calibration | FL reference images FOV B | 10/30/2019 04:17:49 | 8 | 2 | 6.6 | 4 |
| PK20191029161506_013 | 640 | ND3 | Reflective | PKI | Calibration | FL reference images FOV B | 10/30/2019 04:18:02 | 8 | 1 | 6.6 | 8 |
| PK20191029161506_014 | 640 | ND3 | Reflective | PKI | Calibration | FL reference images FOV B | 10/30/2019 04:18:13 | 4 | 1.5 | 6.6 | 2 |
| PK20191029161506_015 | 675 | ND3 | Reflective | PKI | Calibration | FL reference images FOV B | 10/30/2019 04:18:24 | 4 | 2 | 6.6 | 8 |
| PK20191029161506_016 | 675 | ND3 | Reflective | PKI | Calibration | FL reference images FOV B | 10/30/2019 04:18:35 | 4 | 2 | 6.6 | 4 |
| PK20191029161506_017 | 710 | ND3 | Reflective | PKI | Calibration | FL reference images FOV B | 10/30/2019 04:18:45 | 2 | 1 | 6.6 | 8 |
| PK20191029161506_018 | 710 | ND3 | Reflective | PKI | Calibration | FL reference images FOV B | 10/30/2019 04:19:02 | 4 | 1.5 | 6.6 | 4 |
| PK20191029161506_019 | 745 | ND3 | Reflective | PKI | Calibration | FL reference images FOV B | 10/30/2019 04:19:12 | 4 | 1 | 6.6 | 8 |
| PK20191029161506_020 | 745 | ND3 | Reflective | PKI | Calibration | FL reference images FOV B | 10/30/2019 04:19:22 | 2 | 3 | 6.6 | 4 |

| | | | | | | | | | | | | |
|---|---|---|---|---|---|---|---|---|---|---|---|---|
| PKI20191030062323_001 | 430 | ND3 | Reflective | PKI | | | 10/30/2019 18:23:37 | 8 | 1 | 13.4 | 1 |
| PKI20191030062323_002 | 430 | ND3 | Reflective | PKI | | | 10/30/2019 18:23:49 | 16 | 5 | 13.4 | 1 |
| PKI20191030062323_003 | 465 | ND3 | Reflective | PKI | | | 10/30/2019 18:24:03 | 16 | 1 | 13.4 | 8 |
| PKI20191030062323_004 | 465 | ND3 | Reflective | PKI | | | 10/30/2019 18:24:13 | 16 | 3 | 13.4 | 2 |
| PKI20191030062323_005 | 500 | ND3 | Reflective | PKI | | | 10/30/2019 18:24:25 | 16 | 1 | 13.4 | 8 |
| PKI20191030062323_006 | 500 | ND3 | Reflective | PKI | | | 10/30/2019 18:24:34 | 16 | 3 | 13.4 | 4 |
| PKI20191030062323_007 | 535 | ND3 | Reflective | PKI | | | 10/30/2019 18:24:48 | 8 | 3 | 13.4 | 8 |
| PKI20191030062323_008 | 535 | ND3 | Reflective | PKI | | | 10/30/2019 18:25:00 | 8 | 3 | 13.4 | 2 |
| PKI20191030062323_009 | 570 | ND3 | Reflective | PKI | | | 10/30/2019 18:25:13 | 8 | 3 | 13.4 | 8 |
| PKI20191030062323_010 | 570 | ND3 | Reflective | PKI | | | 10/30/2019 18:25:27 | 8 | 1 | 13.4 | 4 |
| PKI20191030062323_011 | 605 | ND3 | Reflective | PKI | | | 10/30/2019 18:25:40 | 8 | 2 | 13.4 | 8 |
| PKI20191030062323_012 | 605 | ND3 | Reflective | PKI | | | 10/30/2019 18:25:53 | 16 | 1 | 13.4 | 4 |
| PKI20191030062323_013 | 640 | ND3 | Reflective | PKI | | | 10/30/2019 18:26:02 | 8 | 2 | 13.4 | 8 |
| PKI20191030062323_014 | 640 | ND3 | Reflective | PKI | | | 10/30/2019 18:26:15 | 16 | 1 | 13.4 | 4 |
| PKI20191030062323_015 | 675 | ND3 | Reflective | PKI | | | 10/30/2019 18:26:25 | 8 | 1 | 13.4 | 8 |
| PKI20191030062323_016 | 675 | ND3 | Reflective | PKI | | | 10/30/2019 18:26:36 | 8 | 1 | 13.4 | 4 |
| PKI20191030062323_017 | 710 | ND3 | Reflective | PKI | | | 10/30/2019 18:26:48 | 4 | 1 | 13.4 | 8 |
| PKI20191030062323_018 | 710 | ND3 | Reflective | PKI | | | 10/30/2019 18:26:58 | 4 | 1 | 13.4 | 4 |
| PKI20191030062323_019 | 745 | ND3 | Reflective | PKI | | | 10/30/2019 18:27:08 | 2 | 2 | 13.4 | 8 |
| PKI20191030062323_020 | 745 | ND3 | Reflective | PKI | | | 10/30/2019 18:27:26 | 4 | 1 | 13.4 | 4 |

| | | | | | | | | | | | |
|---|---|---|---|---|---|---|---|---|---|---|---|
| PKI20191030063821_001 | 430 | ND3 | Reflective | PKI | Calibration | FL reference images FOV D | 10/30/2019 18:38:36 | 8 | 2 | 22.8 | 1 |
| PKI20191030063821_002 | 430 | ND3 | Reflective | PKI | Calibration | FL reference images FOV D | 10/30/2019 18:38:49 | 16 | 12 | 22.8 | 1 |
| PKI20191030063821_003 | 465 | ND3 | Reflective | PKI | Calibration | FL reference images FOV D | 10/30/2019 18:39:10 | 16 | 4 | 22.8 | 8 |
| PKI20191030063821_004 | 465 | ND3 | Reflective | PKI | Calibration | FL reference images FOV D | 10/30/2019 18:39:23 | 16 | 5 | 22.8 | 2 |
| PKI20191030063821_005 | 500 | ND3 | Reflective | PKI | Calibration | FL reference images FOV D | 10/30/2019 18:39:36 | 16 | 1 | 22.8 | 4 |
| PKI20191030063821_006 | 500 | ND3 | Reflective | PKI | Calibration | FL reference images FOV D | 10/30/2019 18:39:46 | 16 | 3 | 22.8 | 2 |
| PKI20191030063821_007 | 535 | ND3 | Reflective | PKI | Calibration | FL reference images FOV D | 10/30/2019 18:39:58 | 8 | 4 | 22.8 | 4 |
| PKI20191030063821_008 | 535 | ND3 | Reflective | PKI | Calibration | FL reference images FOV D | 10/30/2019 18:40:12 | 16 | 3 | 22.8 | 2 |
| PKI20191030063821_009 | 570 | ND3 | Reflective | PKI | Calibration | FL reference images FOV D | 10/30/2019 18:40:24 | 8 | 2 | 22.8 | 4 |
| PKI20191030063821_010 | 570 | ND3 | Reflective | PKI | Calibration | FL reference images FOV D | 10/30/2019 18:40:37 | 16 | 1 | 22.8 | 2 |
| PKI20191030063821_011 | 605 | ND3 | Reflective | PKI | Calibration | FL reference images FOV D | 10/30/2019 18:40:47 | 8 | 3 | 22.8 | 8 |
| PKI20191030063821_012 | 605 | ND3 | Reflective | PKI | Calibration | FL reference images FOV D | 10/30/2019 18:41:00 | 8 | 4 | 22.8 | 2 |
| PKI20191030063821_013 | 640 | ND3 | Reflective | PKI | Calibration | FL reference images FOV D | 10/30/2019 18:41:15 | 8 | 1 | 22.8 | 4 |
| PKI20191030063821_014 | 640 | ND3 | Reflective | PKI | Calibration | FL reference images FOV D | 10/30/2019 18:41:26 | 8 | 1 | 22.8 | 2 |
| PKI20191030063821_015 | 675 | ND3 | Reflective | PKI | Calibration | FL reference images FOV D | 10/30/2019 18:41:38 | 8 | 1 | 22.8 | 8 |
| PKI20191030063821_016 | 675 | ND3 | Reflective | PKI | Calibration | FL reference images FOV D | 10/30/2019 18:41:50 | 8 | 1 | 22.8 | 2 |
| PKI20191030063821_017 | 710 | ND3 | Reflective | PKI | Calibration | FL reference images FOV D | 10/30/2019 18:42:01 | 4 | 1 | 22.8 | 4 |
| PKI20191030063821_018 | 710 | ND3 | Reflective | PKI | Calibration | FL reference images FOV D | 10/30/2019 18:42:11 | 8 | 2 | 22.8 | 4 |
| PKI20191030063821_019 | 745 | ND3 | Reflective | PKI | Calibration | FL reference images FOV D | 10/30/2019 18:42:24 | 4 | 1 | 22.8 | 4 |
| PKI20191030063821_020 | 745 | ND3 | Reflective | PKI | Calibration | FL reference images FOV D | 10/30/2019 18:42:35 | 8 | 2 | 22.8 | 4 |

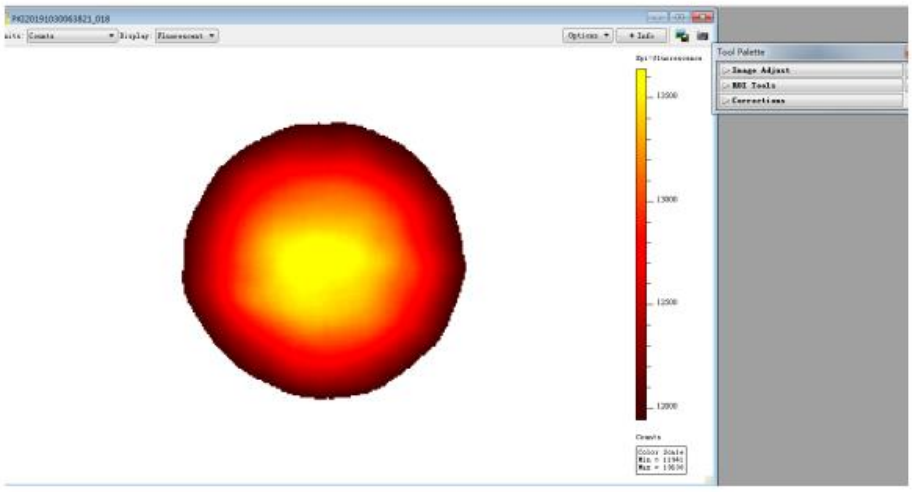


图 38

23. 测试内容：此仪器的摄像头经过校准。

实际测试结果：如图 35-38 所示，此仪器的摄像头经过校准。测试结果符合参数性能指标要求，满足实验需求。


图 39

图 40

24. 图 39-40 是免疫缺陷小鼠成像专用模块，带有 HEPA 过滤膜，用于免疫缺陷型小鼠的隔离成像。


**图 41**

**25.图 41 为 CT 拍摄界面**

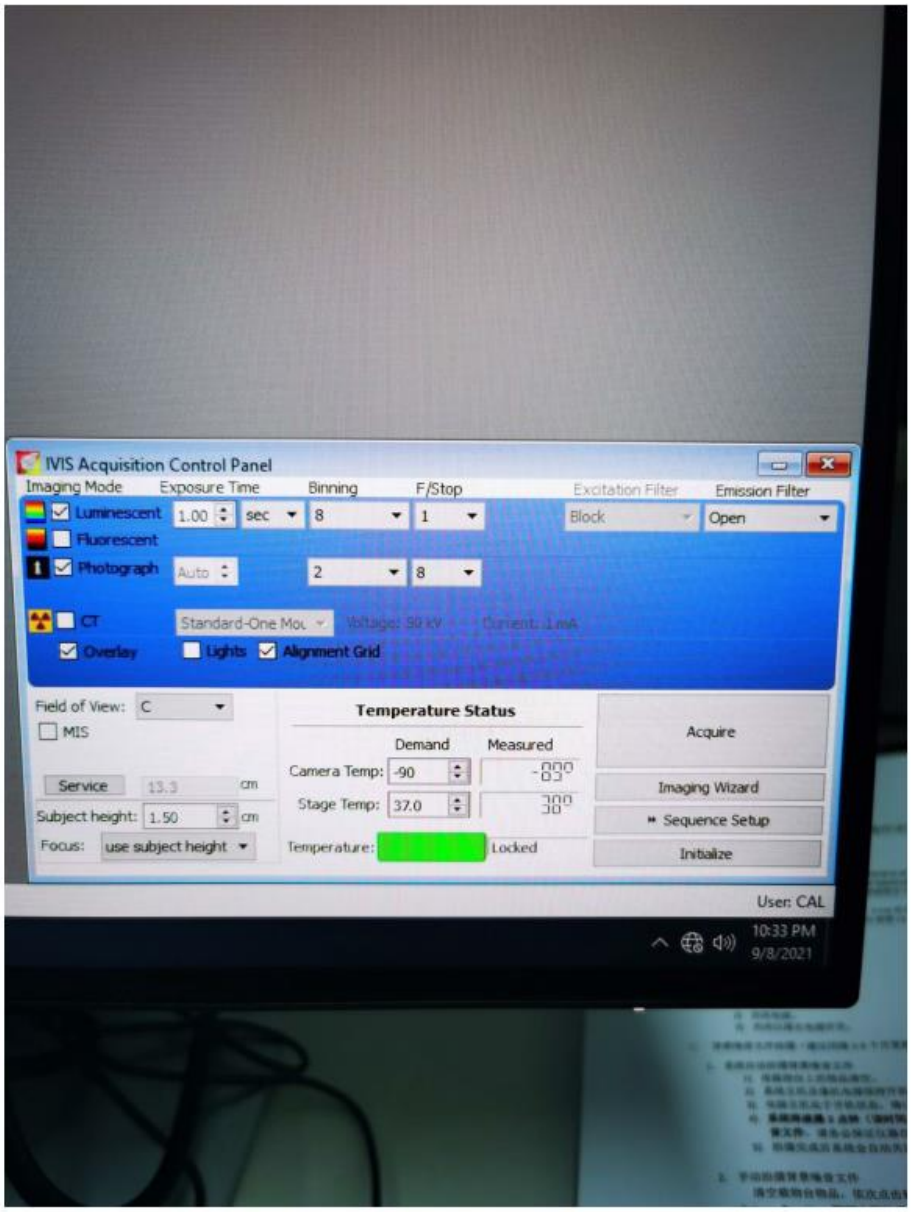


图 42

26.图 42 为 CT 拍摄完成

27.用 CT 拍摄小鼠肠道肿瘤

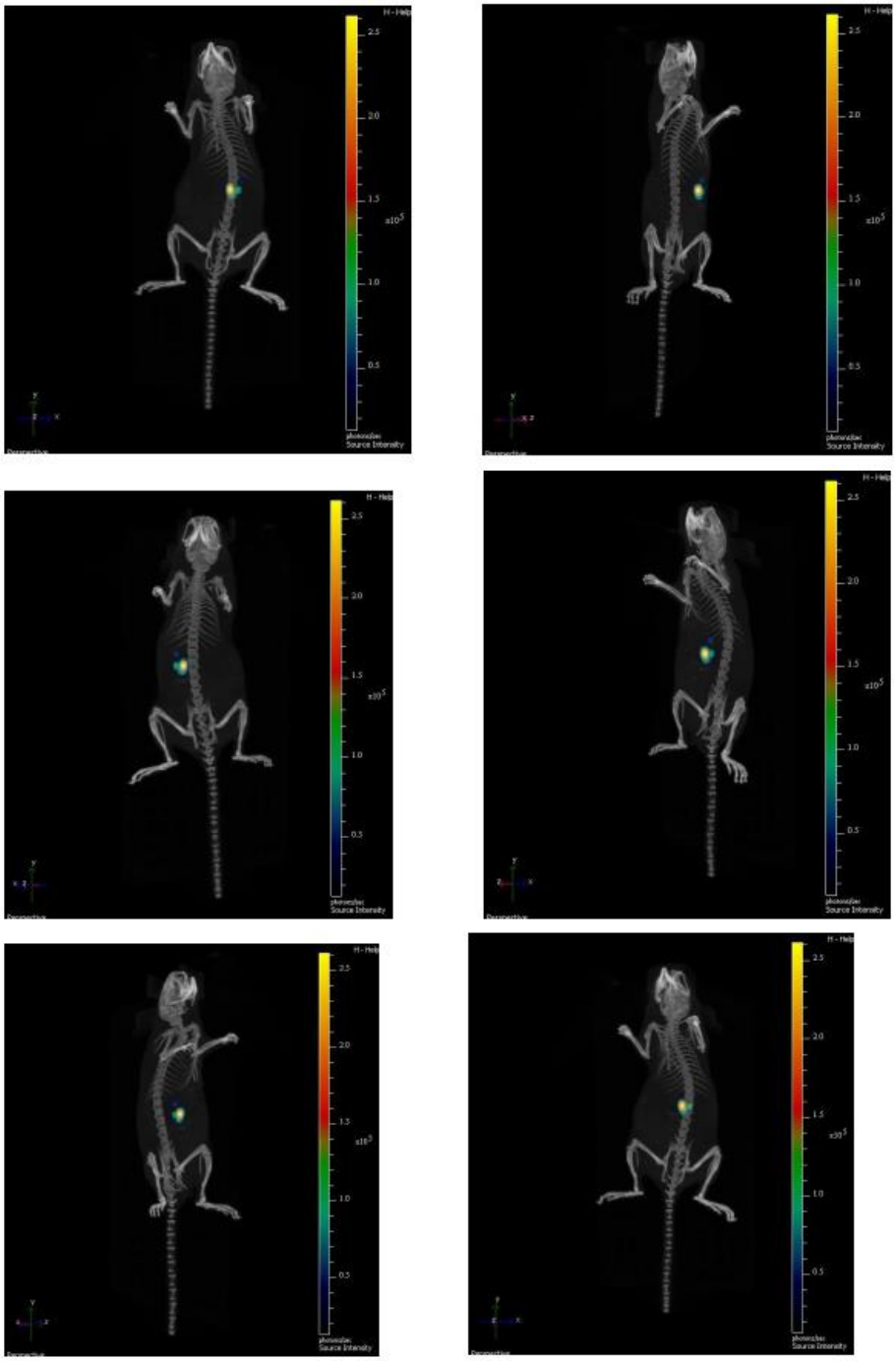

39

28.CT 拍摄小鼠肝癌

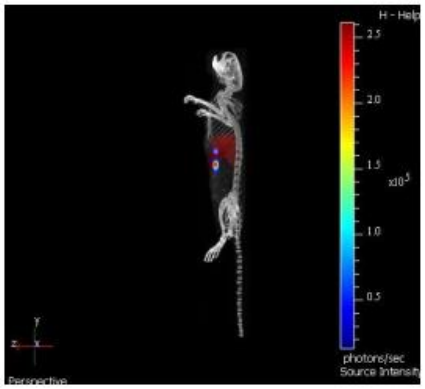
H - Help
2.5
2.0
1.5
x10^5
1.0
0.5
photons/sec
Source Intensity
Perspective

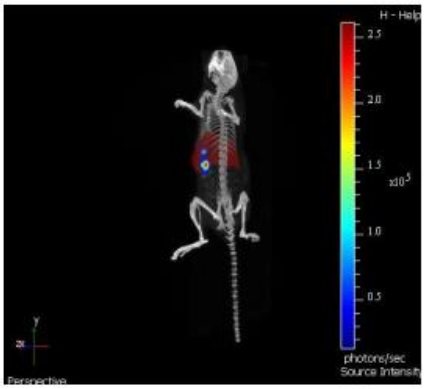
H - Help
2.5
2.0
1.5
x10^5
1.0
0.5
photons/sec
Source Intensity
Perspective

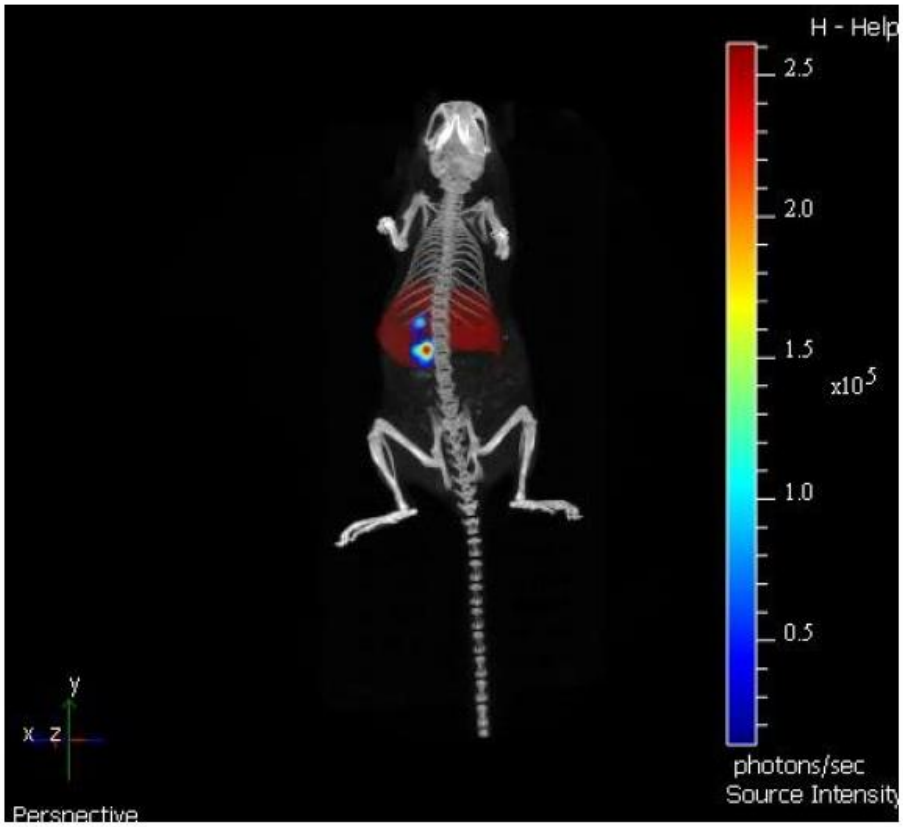
H - Help
2.5
2.0
1.5
x10^5
1.0
0.5
photons/sec
Source Intensity
y
x z
Perspective

29 肿瘤转移

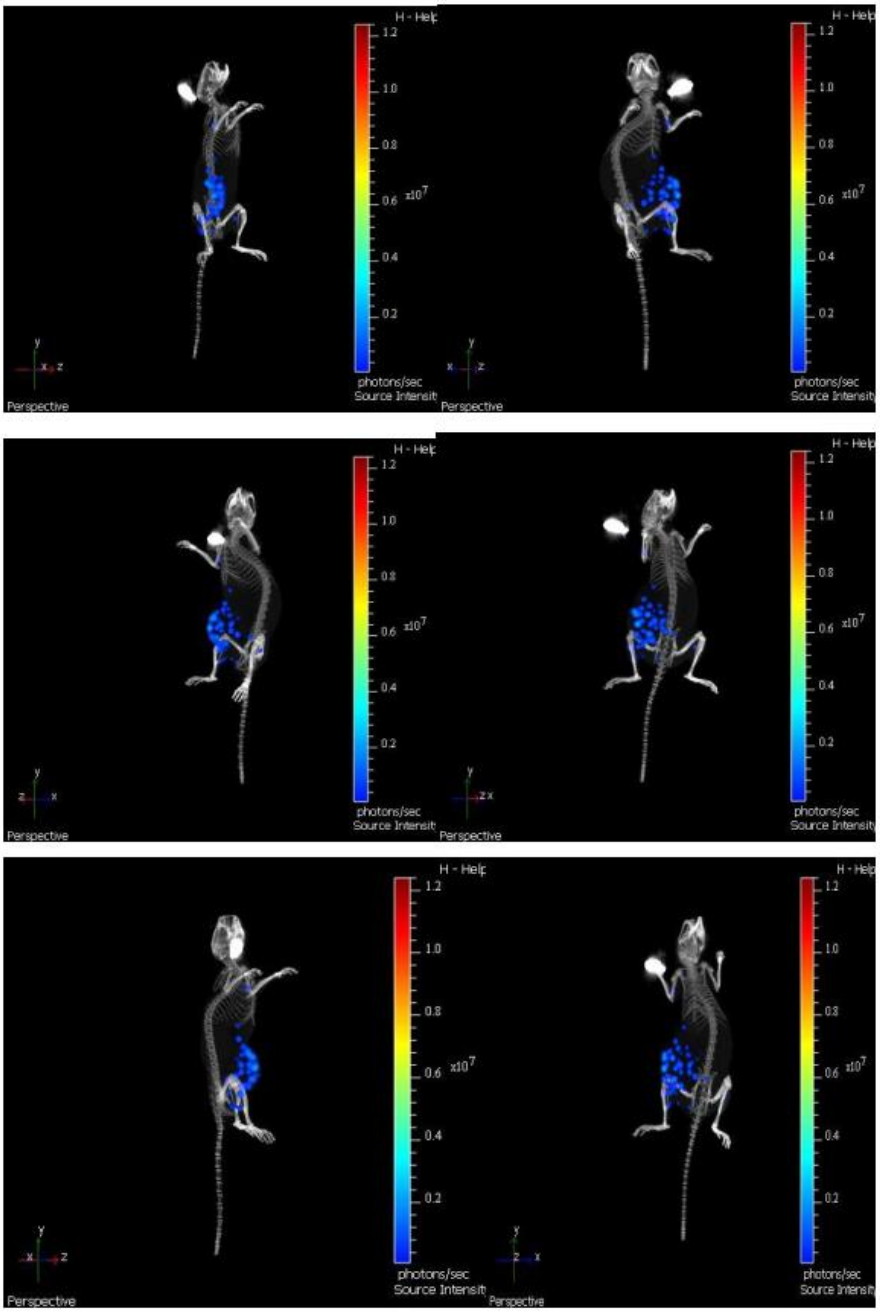
H - Help
1.2
1.0
0.8
0.6
x10^7
0.4
0.2
photons/sec
Source Intensit
Perspective

# 3.2 双人生物安全柜性能测试报告

ThermoFisher SCIENTIFIC

赛默飞世尔（苏州）仪器有限公司

WI-7.5.3-01F

生物安全柜测试报告

型号 1389　　序列号：1389321022523

测试依据 8070-12-001
测试日期 26/02/2021

| 编号 | 基本测试 | 测试方法 | 标准要求 | 测试结果 | 测试人 |
|---|---|---|---|---|---|
| 1 | 柜体防泄漏测试 | 肥皂泡法 | 无气泡产生 | 通过 | 吉恒章 |
| 2 | 高效过滤器完整性测试<br>制造商：Camfil<br>序列号：249-20208214929/194-20218008369<br>测试设备：Photometer<br>供气过滤器尺寸(Inch) 18×72×3.7<br>排气过滤器尺寸(Inch) 18×36×4.6 | 扫描检测<br>压降 80 Pa<br>压降 70 Pa | 泄漏率≤0.01%<br>流量 1350 m3/h<br>流量 680 m3/h | 通过 | 吉恒章 |
| 3 | UV灯测试 | 调整试验法 | 前窗关闭时可用 | 通过 | 吉恒章 |
| 4 | 前窗操作口区域 | 调整位置测试 | 10"+0.25"/-0.75" | 通过 | 吉恒章 |
| 5 | 照明灯开/关测试 | 开/关试验 | 正常操作 | 通过 | 吉恒章 |

| | 电气安全性测试 | 测试方法/设备 | 标准要求 | 测试结果 | 测试人 |
|---|---|---|---|---|---|
| 6 | 接地电阻测试 | 25A/60秒 | <100mΩ | 72.4 | 吉恒章 |
| 7 | 耐压测试 | 2200VDC/2s上升，2s稳定 | <6000uA,无击穿 | 1.2 u | 吉恒章 |
| 8 | 插座极性检测 | 极性插座检测器 | 正常操作 | 通过 | 吉恒章 |
| 9 | 满负荷电流测试 | 钳形电流表 | 测试结果加5A | 6.3 A | 吉恒章 |

| | 流入气流测试 | 测试方法 | 标准要求 | 测试结果 | 测试人 |
|---|---|---|---|---|---|
| 10 | 流入气流测试 | 风量计法 | 100～110LFPM | 通过 | 吉恒章 |
| | 测试设备：风量计 | | | | |
| | 控制参数S2设定值：72 | (<90) | | | |
| | 流入流量(排气流量)：515 | Cu. ft | | | |
| | 前窗开口面积：4.917 | Sq. ft | | | |
| | 流入气流速度：105 | ft/min | | | |

| | 下降气流测试 | 测试方法 | 标准要求 | 测试结果 | 测试人 |
|---|---|---|---|---|---|
| 11 | 下降气流测试 | 直接流速测量法 | 参见标准6.9 | 通过 | 吉恒章 |

测试设备：热式风速仪
当前环境温度值：22.8 °C = 73.04 °F
当前大气压力值：1017 mbar = 1.017 bar
控制参数S1设定值：53
单位：ft/min

| | | | | | | | | | | |
|---|---|---|---|---|---|---|---|---|---|---|
| 61 | 58 | 60 | 62 | 62 | 64 | 66 | 63 | 59 | 60 | 58 |
| 60 | 59 | 61 | 61 | 65 | 63 | 64 | 63 | 60 | 62 | 61 |
| 57 | 59 | 62 | 63 | 64 | 67 | 66 | 64 | 64 | 64 | 57 |

平均下降流速：61.79 ft/min　　流速最大偏差：5.21 ft/min
修正下降流速：61 ft/min　　可接受偏差：± 16 ft/min
流速平均值：通过　　流场均匀性：通过

| | 其他测试 | 测试方法 | 标准要求 | 测试结果 | 测试人 |
|---|---|---|---|---|---|
| 12 | 气流烟雾模式测试 | 观察烟雾法 | 参见标准6.11 | 通过 | 吉恒章 |
| | *以下测试项目进行1/10抽样测试 | | | | |
| 13 | 噪声测试 | 噪声计法<br>背景噪音≤57dBA | ≤67dBA | N/A | 请选择 |
| 14 | 振动测试 | 振动仪 | ≤0.0002" RMS(5μm) | N/A | 请选择 |
| 15 | 光照度测试 | 照度计（每点≥430lx<br>背景照度平均值110±50lx） | 平均值≥650lx | N/A | 请选择 |

打印报告人签名：JA2

DOC NO.: 8070-10-004
Version: 03

Effective date:05/20/2020

Page 1 of 1

# 3.3 脉动真空灭菌器性能测试报告

白象医疗
BAIXIANG MEDICAL

# 脉动真空灭菌器

# 性
# 能
# 测
# 试
# 报
# 告

用户：郑州大学基础医学院　　地址：郑州市高新区科学大道 100 号

仪器品牌：北京白象　　仪器型号：SH-360

测试工程师：王福平　　日期：2021 年 3 月 17 日

# 主要性能测试报告

| 序号 | 合同要求指标 | 实际测试指标 | 是否符合要求 | 备注 |
|---|---|---|---|---|
| 1 | 脉动次数：3 次，0～99 次可调 | 脉动次数：3 次，0～99 次可调（图 1-2） | 符合 | |
| 2 | 灭菌时间：121℃ 20 分钟，134℃ 5 分钟，0～180 分钟可设 | 灭菌时间：121℃ 20 分钟，134℃ 5 分钟，0～180 分钟可设（图 3-4） | 符合 | |
| 3 | 干燥时间：10 分钟，0～180 分钟可设 | 干燥时间：10 分钟，0～180 分钟可设（图 5） | 符合 | |
| 4 | 密封门：双扉机动门，能实现前后“密封互锁”，能使前后门安装连锁，而且还能实现供应室无菌区和污染区的完全隔离 | 双扉机动门，能实现前后“密封互锁”，能使前后门安装连锁，而且还能实现供应室无菌区和污染区的完全隔离（图 6） | 符合 | |
| 5 | 保温措施：夹套与内室温度自动控制，保证灭菌效果，采用非岩棉保温措施 | 保温措施：夹套与内室温度自动控制，保证灭菌效果，采用非岩棉保温措施（图 7） | 符合 | |
| 6 | 灭菌程序：设有织物灭菌、器械灭菌、液体灭菌、B-D 测试、泄漏测试、干燥、自定义 1. 自定义 2 等灭菌程序 | 灭菌程序：设有织物灭菌、器械灭菌、液体灭菌、B-D 测试、泄漏测试、干燥、自定义 1. 自定义 2 等灭菌程序（图 8） | 符合 | |
| 7 | 蒸汽来源：内置蒸汽发生器 | 蒸汽来源：内置蒸汽发生器（图 9） | 符合 | |
| 8 | 测试内容真空保压测试（泄露检测） | 测试内容真空保压测试（泄露检测） | 符合 | |

工程师确认签字：孙福平　　用户确认签字：江水

日期：2021 年 3 月 7 日　　日期：2021 年 3 月 7 日

白象医疗
BAIXIANG MEDICAL

编号：BX-ZJ-16-4.2-2-3

| 设备名称 | 脉动真空蒸汽灭菌器 | 型　号 | HS-360 |
|---|---|---|---|
| 产品批号 | 0360JNPP2101030003 | 生产日期 | 2021 年 01 月 07 日 |
| 产品 TS 批号 | 11362012-222 | ZFQ（TS）批号 | 252011-197 |
| 检验依据 | GB8599-2008/GB4793.1-2007/GB150-2011/产品作业指导书 | | |

| 检验项目 | | 检　验　要　求 | | | 检验结果 |
|---|---|---|---|---|---|
| 1 | 外 观 | 平整光洁、无明显划痕、擦伤、电镀件表面光亮 | | | ☑OK ☐NG |
| 2 | 标识 | 清楚齐全准确 | 设备安全警示标识 | 当心夹手、当心高温、必须接地、当心触电 | ☑OK ☐NG |
| | | | 设备铭牌 | 型号、生产批号、日期 | ☑OK ☐NG |
| 3 | 密封 | 工作时无蒸汽泄漏现象 | | 管路组件无泄漏蒸汽 | ☑OK ☐NG |
| | | | | 灭菌室无泄漏蒸汽 | ☑OK ☐NG |
| | | | | 门密封组件无泄漏蒸汽 | ☑OK ☐NG |
| 4 | 程序显示 | P1～P8 八种功能程序 | | P1～P8 程序运行正常 | ☑OK ☐NG |
| | | P1～P8 八种程序参数调整 | | 八种程序参数编辑自如 | ☑OK ☐NG |
| 5 | 模拟故障提示 | 蒸汽泄漏、真空度、门未关闭等异常自动提示并结束灭菌工作 | | 蒸汽泄漏异常自动报警 | ☑OK ☐NG |
| | | | | 真空度异常自动报警 | ☑OK ☐NG |
| | | | | 门系统未到位自动报警 | ☑OK ☐NG |
| 6 | 温度 | 温度是否达到 132℃、134℃ | | 自动达到 132℃、134℃ | ☑OK ☐NG |
| 7 | 灭菌效果监测 | B-D 测试 | | BD 测试指示物变色均匀 | ☑OK ☐NG |
| | | 生物指示物灭菌测试 | | 培养 48 小时无细菌生长 | ☑OK ☐NG |
| | | 化学指示卡（条）测试 | | 灭菌后符合合格指示色 | ☑OK ☐NG |
| 8 | 附件 | 齐全、准确 | | 说明书、合格证等资料 | ☑OK ☐NG |
| | | | | 配置附件 | ☑OK ☐NG |
| 9 | 包装 | 包装规则整齐，文字清晰准确 | | | ☑OK ☐NG |
| 检验结论 | | 检验合格，允许出厂。 | | | |

| 检验员 | 李　松 | 日期 | 2021 年 01 月 07 日 |
|---|---|---|---|
| 质检部经理 | 唐宏强 | 日期 | 2021 年 01 月 07 日 |

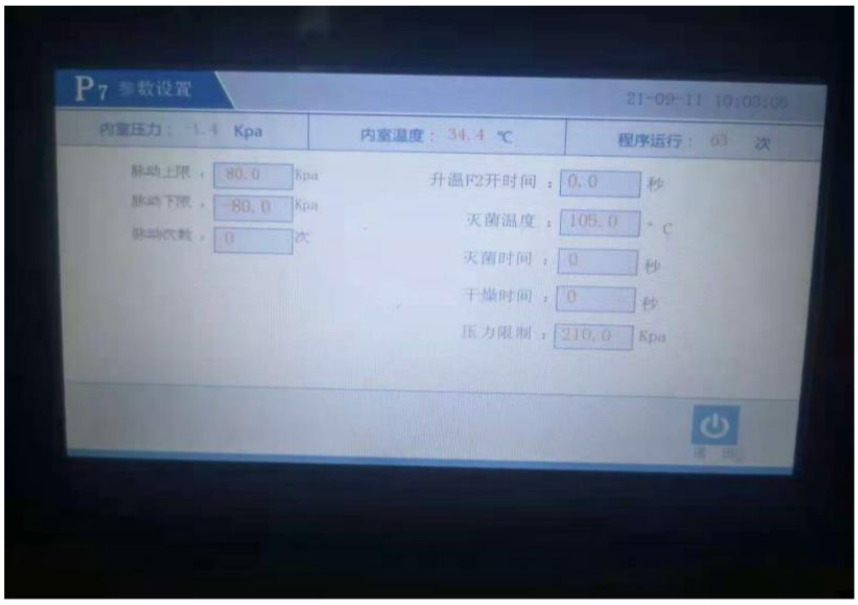


图-1

图 1 测试内容脉动次数下限 0 次的时候灭菌温度为 105°

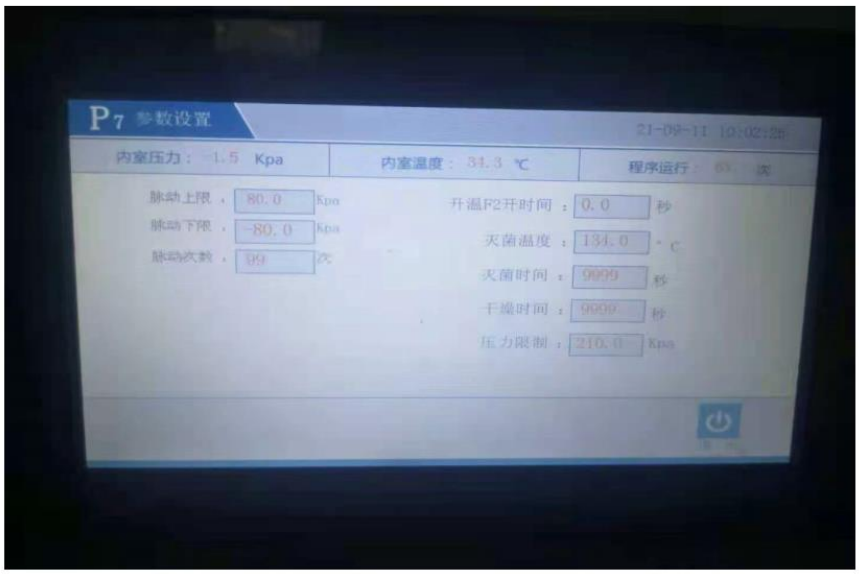


图 2

图 2 测试内容脉动次数上限 99 次的时候灭菌温度为 134°，0-180 分钟可设。

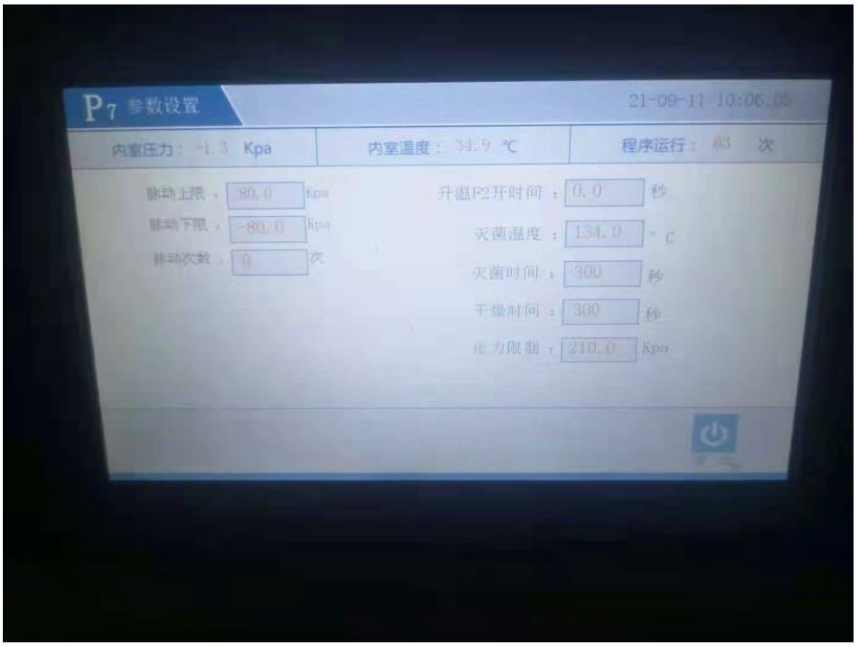


图 3

图 3 测试内容灭菌温度 134°的时候灭菌时间为 5 分钟。0-180 分钟可设。

图 4

图 4 测试内容灭菌温度 121° 的时候灭菌时间为 20 分钟。


图 5

图 5 测试内容，干燥时间：10 分钟，0～180 分钟可设。


图 6

图 6 测试内容，双扉机动门，能实现前后“密封互锁”，能使前后门安装连锁，而且还能实现供应室无菌区和污染区的完全隔离。


图 7

图 7 测试内容夹套与内室温度自动控制，保证灭菌效果，采用非岩棉保温措施。


图 8

图 8 测试内容灭菌程序：设有织物灭菌、器械灭菌、液体灭菌、B-D 测试、泄漏测试、干燥、自定义 1.自定义 2 等灭菌程序。

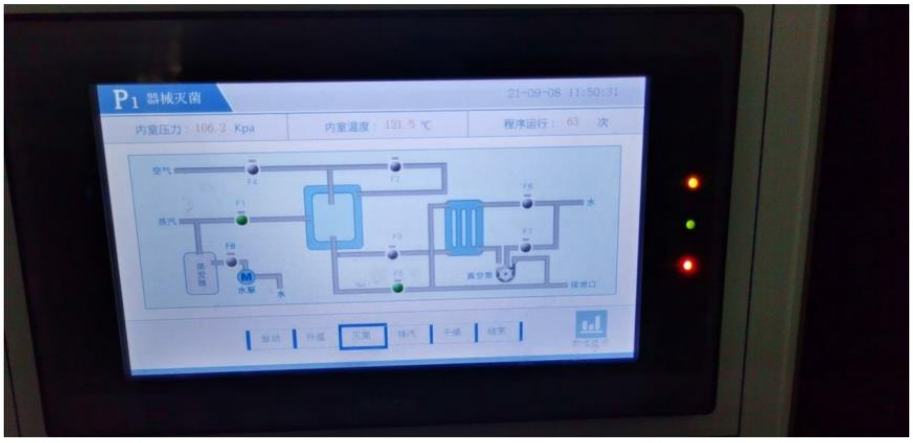


图 9

图 9 测试内容，蒸汽来源：内置蒸汽发生器。

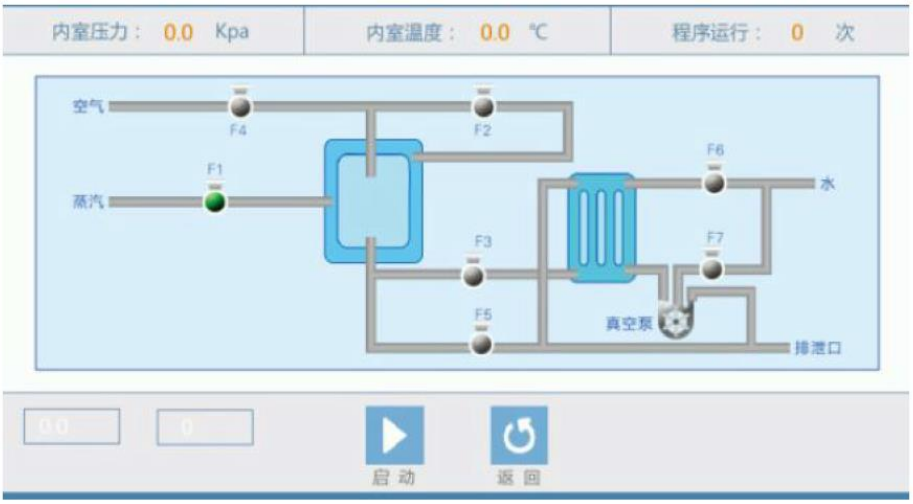


图 10

图 10 测试内容真空保压测试（泄露检测）

图 10


图 11

图 11 测试内容，自选程序可以设置数值。

# 4.设备培训报告

## 4.1 3D 断层多功能活体光学/CT 成像系统培训报告

PerkinElmer
For the Better

3D 断层多功能活体光学/CT 成像系统

**IVIS Spectrum CT**

**培**

**训**

**记**

**录**

客户服务工程师 ： 袁举现、郝盼

使用人：郑州大学基础医学院　　培训日期：2021.8.3

地址：郑州大学基础医学院 533 房间

联系人：江冰　　联系电话：13051575129

供应商：广州市诚屹进出口有限公司　　联系人：黄意

联系电话：17728161724

培训项目：1. 回顾客户仪器安装的性能情况及环境情况

2. 仪器的组成介绍

3. 简述仪器特点及基本工作原理

4. 说明正确的开机顺序及安全操作

5.演示如何启动仪器软件

6. 说明如何进行一个简单的样品拍照

7.简单图形窗口基本功能

8.说明关机程序

9.说明仪器出现故障时应采取的措施及报修步骤

10. 麻醉系统的使用操作

11. 生物发光和荧光的 2D 反射法拍照和结果分析

12.用光谱拆分方法做荧光的 2D 拍照及分析

13.生物发光和荧光的 3D 拍照及结果分析

14. 用实验小鼠做演示实验

培训员：袁举现、郝盼

学习人员：李兵 刘国 葛梦月 张帅兵 马震玉

学习人员意见：经过培训，受训人员已掌握仪器运行原理、各设备功能和仪器操作规程，并已掌握软件的使用方法和设备日常维护及保养，对出现简单故障清排除方法，对以后工作操作有很大帮助。

完成日期：2021 年 8 月 3 日

培训工程师签字确认：袁举现 郝盼　　用户代表签字确认：江水

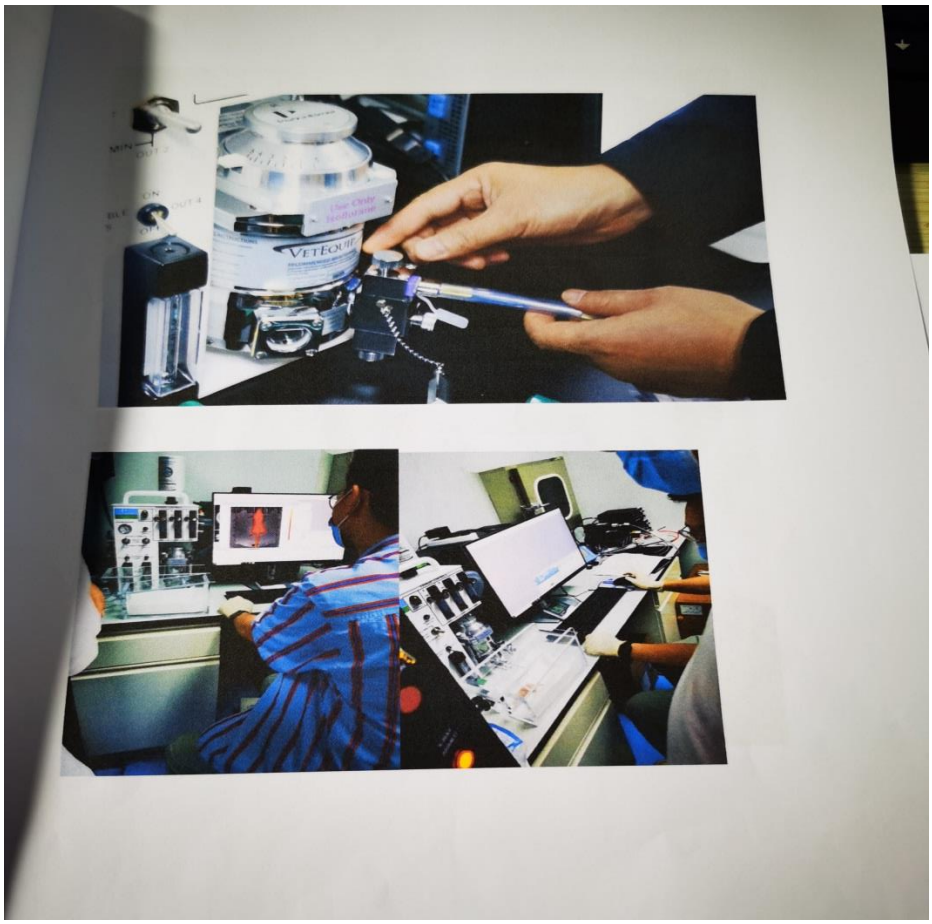
VETEQUIP

# 4.2 双人生物安全柜培训报告

双人生物安全柜

Thermo Scientific/1389

培

训

记

录

客户服务工程师 ： 李明

使用人：郑州大学基础医学院　　培训日期：2021.7.30

地址：郑州大学基础医学院　　房间

联系人：江冰　　联系电话：13051575129

供应商：广州市诚屹进出口有限公司　　联系人：黄意

联系电话：17728161724

培训项目：

一、 设备操作培训

1、线路检查：检查确认插头和电线完好无损，连接正常。

2、开启设备：按住ON键直到听见通风机启动运行的声音，然后状态指示器（LED）会亮起，设备完成启动。（注：从按键到设备响应可能会存在几秒钟的延迟。）

3、设备准备：移动玻璃前窗使处于工作位置（250mm 开口），当绿色指示灯“前窗处于工作位置”亮起时，到达正确位置。（侧导轨上有用以标定前窗较低边缘位置的标记。）等待直到绿色 LED“气流稳定”亮起，此时设备准备完毕，可开始实验操作。

4、实验结束：1）将样品取出后对样品室表面进行清洁和消毒，包括工作托盘和底板及所有附件；2）关闭前窗，空气系统在减少模式下运行（蓝色 LED 亮起），按下控制面板上的 UV 键，直到显示器在 dIS 和剩余消毒时间之间切换。要中断或取消紫外消毒程序，只需按下 UV 键（显示器显示运行时间）。

5、关闭设备：按住 ON（开启）键 5 秒，直到所有 LED 指示灯灭，关闭生物安全柜。在工作间隙或在不需要进行手动操作的长时间实验阶段，可关闭窗口，使设备转换到待机模式。

二、 设备使用与维护注意事项

1、实验过程中，样品应放在工作托盘的指定工作区域，无关物品不要放入样品室。

2、操作过程中只可使用经过清洁和消毒的附件。不要在样品室内放置会引起气流扰动或辐射过多热量的附件

3、不要在样品室内或打开的工作窗前做手、胳膊或身体的快速移动，以免引起

气流扰动；不要在工作托盘的通风槽处阻碍空气循环。

4、每次实验后对样品室进行清洁和消毒。清洁应使用温水混合商用中性洗涤剂，含氯的消毒剂可能会腐蚀设备某些表面，因此只能使用无氯消毒剂！

5、每周应对工作托盘下方区域进行清洁消毒。

学习人员：刘国 新，葛梦月 张帅兵，马赛玉

学习人员意见：熟悉并掌握了生物安全柜的操作方法，运行流程和设备维护注意事项以及安全注意事项，有助于后期试验操作。

完成日期：2021 年 7 月 30 日

培训工程师签字确认：李明　　用户代表签字确认：江 冰

# 4.3 脉动真空灭菌器培训报告

白象医疗
BAIXIANG MEDICAL

脉动真空灭菌器

北京白象/ HS-360

**培**

**训**

**记**

**录**

客户服务工程师 ：王福平

使用人：郑州大学基础医学院　　培训日期：2021.3.17

地址：郑州大学基础医学院　　房间

联系人：江冰　　联系电话：13051575129

供应商：广州市诚屹进出口有限公司　　联系人：黄意

联系电话：17728161724

培训项目：1.灭菌器的使用

2.灭菌器内置蒸汽发生器的使用

3.灭菌器门封条的日常维护，灭菌器机器外表面的日常保养维护

4.蒸汽发生器的日常维护

5.空压机的使用方法

6.空压机的日常维护

7.灭菌器安全阀的日常维护，需要定期校验，每年校验一次

8.压力表的日常维护，需要定期校验，每 6 个月校验一次

9.灭菌器打印记录的保存，以及打印纸的更换安装

10.压力容器遇到突发停水，停电，如何操作。

11.灭菌物品的摆放要求，以及灭菌后物品的存放。

培训工程师：王福平

学习人员：刘同 新 高梦月 张帅兵、马晨玉

学习人员意见：学习了灭菌器的基础知识、操作使用方法和日常维护，对以后试验操作有着极大帮助。

完成日期：2021 年 3 月 17 日

培训工程师签字确认：王福平

用户代表签字确认：江冰